Atmos. Chem. Phys. Discuss., 13, 20611–20676, 2013
www.atmos-chem-phys-discuss.net/13/20611/2013/
doi:10.5194/acpd-13-20611-2013

Atmospheric Chemistry and Physics Discussions

Modelling the chemistry and transport of bromoform within a sea breeze driven convective system during the SHIVA Campaign

P. D. Hamer[1], V. Marécal[1], R. Hossaini[2], M. Pirre[3], N. Warwick[4], M. Chipperfield[2], A. A. Samah[5,6], N. Harris[4], A. Robinson[4], B. Quack[7], A. Engel[8], K. Krüger[7], E. Atlas[9], K. Subramaniam[10], D. Oram[11], E. Leedham[11], G. Mills[11], K. Pfeilsticker[12], S. Sala[8], T. Keber[8], H. Bönisch[8], L. K. Peng[13], M. S. M. Nadzir[14], P. T. Lim[15], A. Mujahid[15], A. Anton[16], H. Schlager[17], V. Catoire[3], G. Krysztofiak[3], S. Fühlbrügge[7], M. Dorf[12], and W. T. Sturges[11]

[1]Centre National de Recherches Météorologiques-Groupe d'étude de l'Atmosphère Météorologique, Météo-France and CNRS, UMR3589, Toulouse, France
[2]The Institute for Climate & Atmospheric, Science, School of Earth and Environment, University of Leeds, Leeds, UK
[3]Laboratoire de Physique et Chimie de l'Environnement et de l'Espace, CNRS and University of Orléans, UMR7328, Orléans, France

[4]Centre for Atmospheric Science, Cambridge University, Chemistry Department, Lensfield Road, Cambridge, CB2 1EW, UK
[5]National Antarctic Research Centre, University of Malaya, Kuala Lumpur 50603, Malaysia
[6]Institute of Ocean & Earth Sciences, University of Malaya, 50603 Kuala Lumpur, Malaysia
[7]GEOMAR, Helmholtz Centre for Ocean Research Kiel, Düsternbrooker Weg 20, 24105, Kiel, Germany
[8]Institute of Atmospheric and Environmental Science, Dept. of Experimental AtmosphericResearch, J. W. Goethe-University Frankfurt am Main, Germany
[9]University of Miami, 4600 Rickenbacker Causeway, Miami, FL 33149, USA
[10]Malaysian Meteorological Department, Headquarter of Malaysian Meteorological Department, Jalan Sultan, 46667 Petaling Jaya, Malaysia
[11]School of Environmental Sciences, University of East Anglia, Norwich Research Park, Norwich, NR4 7TJ, UK
[12]Institute of Environmental Physics, Ruprecht-Karls-Universität Heidelberg, Im Neuenheimer Feld 229, 69120 Heidelberg, Germany
[13]Malaysian Meteorological Department, Ketua Stesen GAW Lembah Danum, Jabatan Meteorologi Malaysia, Cawangan Sabah, Lapangan Terbang Wakuba Tawau, Peti Surat 60109, 91011 Tawau, Sabah, Malaysia
[14]School of Environmental and Natural Resource Sciences, Faculty of Science and Technology, Universiti Kebangsaan Malaysia, 43600 Bangi, Selangor, Malaysia
[15]Department of Aquatic Science, Universiti Malaysia Sarawak, 94300 Kota Samarahan, Sarawak Malaysia
[16]Borneo Marine Research Institute, Universiti Malaysia Sabah, Jalan UMS, 88400 Kota Kinabalu, Sabah, Malaysia
[17]Deutsches Zentrum für Luft- und Raumfahrt (DLR), Institut für Physik der Atmosphäre, Atmosphärische Spurenstoffe, Münchner Straße 20, 82234 Oberpfaffenhofen-Wessling, Germany

Received: 31 May 2013 – Accepted: 26 July 2013 – Published: 7 August 2013

Correspondence to: P. D. Hamer (paul.hamer@meteo.fr)

Published by Copernicus Publications on behalf of the European Geosciences Union.

Abstract

We carry out a case study of the transport and chemistry of bromoform and its product gases (PGs) in a sea breeze driven convective episode on 19 November 2011 along the North West coast of Borneo during the "Stratospheric ozone: Halogen Impacts in a Varying Atmosphere" (SHIVA) campaign. We use ground based, ship, aircraft and balloon sonde observations made during the campaign, and a 3-D regional online transport and chemistry model capable of resolving clouds and convection explicitly that includes detailed bromine chemistry. The model simulates the temperature, wind speed, wind direction fairly well for the most part, and adequately captures the convection location, timing, and intensity. The simulated transport of bromoform from the boundary layer up to 12 km compares well to aircraft observations to support our conclusions. The model makes several predictions regarding bromine transport from the boundary layer to the level of convective detrainment (11 to 12 km). First, the majority of bromine undergoes this transport as bromoform. Second, insoluble organic bromine carbonyl species are transported to between 11 and 12 km, but only form a small proportion of the transported bromine. Third, soluble bromine species, which include bromine organic peroxides, hydrobromic acid (HBr), and hypobromous acid (HOBr), are washed out efficiently within the core of the convective column. Fourth, insoluble inorganic bromine species (principally Br_2) are not washed out of the convective column, but are also not transported to the altitude of detrainment in large quantities. We expect that Br_2 will make a larger relative contribution to the total vertical transport of bromine atoms in scenarios with higher $CHBr_3$ mixing ratios in the boundary layer, which have been observed in other regions. Finally, given the highly detailed description of the chemistry, transport and washout of bromine compounds within our simulations, we make a series of recommendations about the physical and chemical processes that should be represented in 3-D chemical transport models (CTMs) and chemistry climate models (CCMs), which are the primary theoretical means of estimating the contribution made by $CHBr_3$ and other very short-lived substances (VSLS) to the stratospheric bromine budget.

1 Introduction

The primary contributors to the total stratospheric bromine loading (strat-Br_y) are organic bromine gases. A portion of the strat-Br_y budget is consists of strat-Br_y^{VSLS}, which results from VSLS that contain bromine; VSLS are defined as having a lifetime of less than 6 months (Law and Sturges, 2006). There remain considerable uncertainties for the estimation of strat-Br_y^{VSLS} (Montzka and Reimann, 2011). Observations from various platforms, primarily of BrO, have been used to estimate strat-Br_y^{VSLS}: balloon based instruments estimate $4.1 \pm 2.5\,\mathrm{pmol\,mol^{-1}}$ (Dorf et al., 2006); estimates from satellite retrievals include $\sim 3\,\mathrm{pmol\,mol^{-1}}$ (Sinnhuber, 2005), $\sim 5\,\mathrm{pmol\,mol^{-1}}$ (McLinden, 2010) and up to $\sim 8.4\,\mathrm{pmol\,mol^{-1}}$ (Sioris, 2006). The compiled range for Br_y^{VSLS} based on observations of BrO (i.e. the inorganic derivation) is 6 (3–8) ppt (Montzka and Reimann, 2011). The diversity of observational estimates might be explainable by the varying vertical sensitivities and sampling altitudes of the different methods (Choi et al., 2012), and due to the different values of the $j(BrONO_2)$ / $(k(BrO+NO_2)$ ratio used to estimate strat-Br_y^{VSLS} using the inorganic method (Kreycy et al., 2012). Contemporary studies using global chemistry models estimate a contribution to strat-Br_y^{VSLS} ranging from 1.6 to $3\,\mathrm{pmol\,mol^{-1}}$ (Aschmann et al., 2009), $2.4\,\mathrm{pmol\,mol^{-1}}$ (Hossaini et al., 2010), $\sim 5\,\mathrm{pmol\,mol^{-1}}$ (Aschmann et al., 2010; Liang et al., 2010; Hossaini et al., 2012), to up to 6 to $7\,\mathrm{pmol\,mol^{-1}}$ (Warwick et al., 2006). This diversity of estimates is due to differences in approach, e.g., which VSLS are considered and what assumptions are made. Table 1 summarises the differences in method and assumptions between the different modelling studies. This clearly demonstrates a direct sensitivity between estimated strat-Br_y^{VSLS} and the methodological choices within CTMs and CCMs. Thus,

there is a need to address the validity of these assumptions, which partly represents the motivation for this study. For models to reasonably estimate strat-Br_y^{VSLS} they need to consider a wide range of processes affecting VSLS source gases (SGs) and product gases (PGs): emissions of VSLS, chemistry, transport, dry deposition, and the washout of soluble species. We will now attempt to review these processes and discuss the key uncertainties in studying halogenated VSLS with global models.

VSLS have a largely biogenic and oceanic origin. Measurements of VSLS concentrations in surface ocean water and observed mixing ratios in the atmosphere indicate emissions are larger towards coasts compared to the open ocean (Quack and Wallace, 2003). Of the recognised brominated VSLS, $CHBr_3$ has the largest emissions, is the most reactive, has the shortest atmospheric lifetime, and is contains three bromine atoms. Contemporary global estimates of $CHBr_3$ emissions range between 127 and 600 $Gg\,yr^{-1}$ (Liang et al., 2010; Warwick et al., 2006; Ordóñez et al., 2012; Pyle et al., 2011; Ziska et al., 2013). In addition, a consensus exists that emissions are predominantly distributed in the tropics, but there remains considerable uncertainty regarding the precise spatial distribution of emissions. The performance of the various top-down and bottom-up $CHBr_3$ inventories varies significantly by region, representing a significant source of uncertainty in model estimates of strat-Br_y^{VSLS} (Hossaini et al., 2013).

In addition to the tropics being the region with the largest VSLS emissions, tropical deep convection is the primary mechanism that leads to the transport of tropospheric trace gases and aerosols to the stratosphere. Deep convection can be initiated via two main processes: vertical thermodynamic instabilities, and low level convergence driven by either synoptic or mesoscale motions. Convection, and its associated tracer transport, is represented within CTMs and CCMs by convective parameterisations. The parameterisations represent seasonal variability, precipitation magnitude, and tracer transport well in most regions, but there exist large discrepancies in the important Maritime Continent (MC) (Arteta et al., 2009a; Russo et al., 2011). The MC is a key region for pronounced fast transport of tropospheric air to the stratosphere (Fueglistaler et al., 2005; Krüger et al., 2009). In addition, in all regions, there exist outstanding uncertain-

ties regarding moisture transport to the level of zero radiative heating (LZRH) (Russo et al., 2011). Further, the convective mass fluxes estimated by convective parameterisations are again subject to remaining uncertainties that particularly affect the transport of short-lived tracers within CTMs (Hoyle et al., 2011; Arteta et al., 2009a).

The transport of SGs and PGs to the upper troposphere and lower stratosphere (UTLS) within tropical convective systems, and the consequent injection of SGs and PGs (termed SGI and PGI, respectively) to the stratosphere (Montzka and Reimann, 2011), is affected by gas phase chemistry and photochemistry, aqueous phase chemistry, dry deposition, aqueous phase uptake, and washout, which primarily affect the PGs. Given computational limitations and the array of complex processes controlling strat-Br_y^{VSLS}, previous studies used various assumptions to simplify their simulations. Table 1 highlights the assumptions for the contemporary studies using global chemistry models (Aschmann et al., 2009, 2010; Hossaini et al., 2010, 2012; Liang et al., 2010; Warwick et al., 2006). Of note is the use of fixed and uniform tropical boundary layer mixing ratios of the VSLS, which ignores the inhomogeneities in the spatial and temporal distribution, and the simplified treatment of Br_y washout, which often ignores variations in washout efficiency due to varying solubility for different Br_y components. In addition, all of the studies mentioned above use convective parameterisations to derive the convective mass flux for tracers. Finally, the choice of chemical mechanism presents another source of uncertainty. Hossaini et al. (2010, 2012) represent the state of the art for 3-D CTMs including the organic degradation products of VSLS, but Hossaini et al. (2010) does not speciate the inorganic Br_y. Hossaini et al. (2010) showed that organic PGs make only a minor contribution to strat-Br_y^{VSLS}. The other studies neglect the organic PGs and only Aschmann et al. (2010), in addition to Hossaini et al. (2012), speciates inorganic Br_y into soluble and insoluble forms.

So far, only model studies with smaller spatial domains, with shorter simulation time span, and with only idealised setup have examined VSLS degradation chemistry (both gas and aqueous phase) in high detail (Krysztofiak et al., 2012; Marécal et al., 2012). Krysztofiak et al. (2012) focused on developing and optimising a photochemical mech-

anism for $CHBr_3$ degradation for use within regional models, and it estimated Henry's Law coefficients for some of the organic bromine species within the optimised mechanism. Marécal et al. (2012) implemented the $CHBr_3$ photochemical scheme of Hossaini et al. (2010) in addition to aqueous phase uptake and chemistry based on the Henry's Law coeffecients from Krysztofiak et al. (2012). Using idealised simulations of tropical convective clouds Marécal et al. (2012) highlighted the importance of aqueous phase processes for understanding SG and PG chemistry and transport. In particular, the formation of Br_2 in the aqueous phase and subsequent release into the gas phase was found to make a non-negligible contribution to the upper tropospheric bromine budget:

$$HOBr_{(aq)} + Br^-_{(aq)} + H^+ \rightarrow Br_{2(aq)} + H_2O \quad \text{(R1)}$$

The MC of South East Asia (SEA-MC) represents globally the most important region for deep convection (Liu and Zisper, 2005). Thus, the 2011 November campaign of the EU project SHIVA focused on this region to better understand the transport of VSLS to the stratosphere and their role in ozone (O_3) depletion. The aircraft campaign was based in Miri, Sarawak, Malaysia and involved, aircraft, ship, and ground based observations of chemical and meteorological parameters, and sonde and radar observations of meteorological variables (Pfeilsticker et al., 2013). Over Borneo during the winter monsoon the onset of deep convection is primarily controlled by convergent surface flows that initiate convective upwelling, which can either be synoptically driven (i.e. cold surges) or driven by processes at the mesoscale (i.e. sea breeze convergence) (Houze et al., 1981; Johnson et al., 1982, 2004). Previous attempts to simulate the sea breeze driven convergence and the consequent convection and rainfall in this region at the mesoscale were successful (Dudhia, 1989; Wu et al., 2008). However, global climate models operating on coarser resolutions still systematically fail to fully represent the extent of rainfall resulting from complex diurnal sea breeze circulation patterns over this region (Neale and Slingo, 2003).

One intriguing aspect of the study region is that there is the potential for interactions between marine and polluted urban air masses (von Glasow et al., 2012). We include

two chemical reactions that could lead to interactions between these two types of air mass:

$$HCHO + Br \rightarrow HBr + CO + HO_2 \quad \text{(R2)}$$

$$BrO + NO_2 \rightarrow BrONO_2 \quad \text{(R3)}$$

Marécal et al. (2012) explored the uncertainties in model representations of VSLS chemistry, including multi-phase processes and removal (washout) of soluble products under idealised meteorological conditions using an artificially generated convective event. Marécal et al. (2012) focused only on $CHBr_3$ due to computational limitations and because it is the most abundant and reactive VSLS. In this study we aim to build upon the work of Marécal et al. (2012) focusing again on $CHBr_3$ but with a case study of a well observed convective event off the North West coast of Borneo during the SHIVA campaign at the early stages of the 2011 monsoon on 19 November. We use a regional meteorological model coupled to a gas and aqueous phase chemistry model in conjunction with in-situ, aircraft, sonde, and ship measurements of trace gases and meterological parameters to carry out this case study. Our objectives are:

- To understand the chemistry of $CHBr_3$ and to estimate the chemical budget within a single convective system for all of the different forms of Br-species and to relate this to the uptake and washout efficiency for the various PGs.
- To identify how these processes relate to assumptions currently used within CTMs and CCMs, and indicate how this could affect the conclusions of pre-existing studies.

Section 2 provides an overview of the case study. Section 3 describes the model used, recent developments affecting its development, and its configuration. Section 4 presents our results and includes discussion of the meteorological and chemical simulations. Section 5 discusses our conclusions, recommendations for CTM studies, and future work.

2 Case study overview

Pfeilsticker et al. (2013) (this issue) provides an overview of the SHIVA campaign. On 19 November 2011 the Deutsches Zentrum für Luft- und Raumfahrt (DLR) Falcon aircraft flew two sorties from Miri, Sarawak. Flight A from 11:10 to 14:40 LT, Flight B from 15:50 to 18:20 LT (Fig. 1). Flight A flew low in the atmosphere below 2 km for most of the flight, but included two short sections up to 8 km. Flight B flew just off the coast of Borneo at an altitude of ∼ 12 km and observed signatures of convective outflow: elevated mixing ratios of carbon monoxide (CO) from the SPIRIT instrument (Guimbaud et al., 2011 and Catoire et al., 2013), and $CHBr_3$ from the GHOST-MS instrument. Figure 2 shows the sections of Flight B where elevated levels of CO ($> 80\,\mathrm{nmol\,mol^{-1}}$ $\mathrm{nmol\,mol^{-1}}$) were observed relative to the observed pervasive background of $\sim 70\,\mathrm{nmol\,mol^{-1}}$ $\mathrm{nmol\,mol^{-1}}$ at 12 km. Observations of CO throughout the campaign indicate very little vertical gradient in the sampled air masses. Thus, enhancements of up to $15\,\mathrm{nmol\,mol^{-1}}$ are therefore indicative of enhanced vertical transport. The elevated levels of CO associated with convective outflow were primarily observed during the flight in a region centred around 115.4° E and 5.8° N, which we henceforth term Region 1. At 12 km at this location the wind blew consistently from 100°, which is part of the general circulation over this region. The convective system was detected by the Malaysian Meteorological Department (MMD) weather radar station at Kota Kinabalu to the East of Region 1 is therefore the cause of the observed convective outflow. Radar rainfall during Flight B indicates that the convective system resided over the ocean and land within 50 km of the western coast of Borneo (Figs. 3 and 4). We term the area where the bulk of the convective rainfall occurs Region 2A (Fig. 2). In addition, Figs. 3 and 4 depict a series of echoes that extend between Region 1 and Region 2A along an East South East axis, which we surmise is rainfall resulting from an out flowing anvil. The occurrence of the event on 19 November and its well observed nature provided the motivation for selecting this day for study. The convection on 19 November was initiated by sea breeze convergence along the western coast of

Borneo. This is generally consistent with the model put forward by Johnson et al. (2004) whereby diurnal sea breezes set up convergence inland and orographic effects due to inland mountains lead to the formation of a propagating thermally driven gravity wave that together cause the development of rain offshore during the late evening. Figure 3 shows the early to mid stages of the convective event indicating that a pattern of heavy rain builds up inland with light and more diffuse rain occurring over the ocean. Not shown is the further development and intensification of the rain offshore after 21:00 LT in the radar rainfall data, which is a further component of the Johnson et al. (2004) conceptual model.

In this study we use the meteorological and chemical data collected during the time period covered by the simulation from the Sonne Research Vessel (RV), local boats, at Bukit Atur, and from the Falcon. We use meteorological parameters collected by the radiosonde launches from Kuching and aboard the RV Sonne, and precipitation rates derived from the MMD weather radar network. All of the data that we use are summarised in Table 2. Figure 1 shows the location of the RV Sonne and local boat cruises, of Bukit Atur, Miri, and Kuching in context relative to the locations of Flights A and B.

3 Model

3.1 Model description

We use the Chemistry-Coupled Aerosol and Tracer Transport model to the Brazilian developments on the Regional Atmospheric Modeling System (C-CATT-BRAMS) (Longo et al., 2013), which is a version of the CATT-BRAMS model (Freitas et al., 2009) coupled on-line with a chemistry model. This system is capable of resolving meteorological processes and the resultant tracer transport and chemistry. C-CATT-BRAMS has its original heritage in the Regional Atmospheric Modeling System version 6 (RAMS) (Walko et al., 2000). RAMS is a fully compressible non-hydrostatic model consistent

with Tripoli and Cotton (1982). RAMS has the ability to run in a nested grid configuration and includes various physical parameterisations to simulate sub-grid scale meteorological processes for turbulence, shallow cumulus convection, deep convection, surface-air exchanges, cloud microphysics, and radiation. BRAMS builds upon RAMS with the inclusion of several modifications that serve to improve the model performance within the tropics, for example: an ensemble implementation of the deep and shallow cumulus convection schemes, a soil moisture initialisation using model prognostication combined with a remote sensing rainfall product, and more realistic surface characteristics for vegetation type derived from the MODIS NDVI product.

The model represents microphysical processes using the single-moment bulk parameterization (Walko et al., 1995) whereby rain, cloud, pristine ice, snow, aggregates, graupel and hail are considered. The radiation scheme used in the model calculates the effects of clouds, hydrometeors, and aerosols upon radiation (Toon et al., 1989). The model considers turbulent mixing using the turbulent kinetic energy (mean kinetic energy per unit mass for eddies in turbulent flow) as a prognostic variable (Mellor and Yamada, 1982).

The chemistry scheme coupled to CATT-BRAMS simulates gas and aqueous phase chemistry, photochemistry, uptake described by Henry's Law, and hydrolysis. Marécal et al. (2012) and Krysztofiak et al. (2012) together provide a detailed overview of the equations describing the chemistry solved by the model. To summarise, the model solves for the chemical loss and production, and for species concentrations, in the gas phase, in cloud particles, and rain droplets considering all of the processes described above. The chemistry scheme couples with the microphysical scheme to estimate how uptake within hydrometeors leads to and affects washout. To this end, the model considers within the bulk microphysical scheme the effects of condensation, evaporation, water vapour deposition, and sedimentation. In addition, the reversible exchange of gases between the gas and aqueous phases is estimated using Henry's Law and accommodation constants. Once within the condensed phase, the model also includes an estimation for the transfer of chemical species from within cloud particles to the different

types of hydrometeor during coalescence and riming, and within the individual types of hydrometeor. Finally, chemical species caught within ice particles are considered to be lost via washout and we assume a retention coefficient of 1 for all species. This assumption is valid since ice particles primarily develop into hail and graupel, which sediment rapidly relative to the retention time of chemical species on their surfaces.

Of particular importance is the $BrONO_2$ hydrolysis reaction within cloud particles and rain droplets that has been added to the chemical scheme. Its mathematical implementation is described by Marécal et al. (2012) in Sect. 2.2. The reaction scheme considers the reaction within cloud particles and rain droplets separately using the mean mass radius and mean mixing ratios for cloud particles and rain droplets from the bulk micro-physical scheme, the thermal velocity, the gas phase diffusivity, and the accommodation coefficient of $BrONO_2$.

3.2 Recent developments

In order for the model to simulate chemical and physical processes associated with $CHBr_3$ degradation chemistry and its transport several important changes had to be made to the model. A photochemical mechanism for the degradation of $CHBr_3$ was developed, tested, and optimised for use in CATT-BRAMS (Krysztofiak et al., 2012). The development of the new mechanism also included the estimation of the most favoured branching ratios for the $XRO_2 + HO_2$ reactions (see Table 1 of Krysztofiak et al., 2012 for more details) using ab initio calculations of the standard reaction enthalpies. Reaction rates were either estimated from the analogous chlorine compounds or via a generalised expression. In addition, to properly simulate the uptake and washout of PGs into cloud particles and rain droplets, Henry's Law coefficients had to be estimated using predictive methods: the bond contribution method, (Meylan and Howard, 1991) and the molecular connectivity index (Nirmalaklandan and Speece, 1988) for the brominated organic peroxides, CBr_3O_2H, $CHBr_2O_2H$, and the brominated carbonyl species, CBr_2O and CHBrO. These new developments were successfully implemented by Marécal et al. (2012). Building on the new mechanism implemented in Marécal

et al. (2012), non-methane hydrocarbon (NMHC) chemistry was added to the chemical mechanism. The NMHC mechanism is a reduced version of the Regional Atmospheric Chemistry Mechanism (Stockwell et al., 1997) called Regional Lumped Atmopsheric Chemical Scheme (ReLACS, Crassier et al., 2000). The full chemical mechanism is described in Appendix A.

To describe $CHBr_3$ emissions we have implemented an emission inventory based on the work of Warwick et al. (2006) and Pyle et al. (2011) (see Fig. 5). The emissions have a 20 km × 20 km resolution, distribute approximately half of the emissions within a 20 km wide coastal band immediately adjoining the coastline and the rest over open ocean, emit ∼ 12 times more in the coastal zone compared to the open ocean, and have a total global emission of 375 Gg yr^{-1}. The Warwick et al. (2006) and Pyle et al. (2011) emissions differ notably from other VSLS emissions inventories in that they use a much finer spatial resolution, and the coastal outline represented most of the islands and land masses within the SEA-MC. These points provide some of the motivation for selecting these emissions, so as to complement the fine spatial resolution of our model simulation. In addition, these emissions have already been validated over this region using ground-based observations (Pyle et al., 2011) and also with aircraft observations (Hossaini et al., 2013). Further, within the 20 km wide coastal band along the northern coast of Borneo, the Warwick et al. (2006) and Pyle et al. (2011) emissions show reasonable agreement with estimates derived from observations (Ziska et al., 2013), and, at a regional scale within the SEA-MC, they compare well to the upper limit for coastal emissions dervied from laboratory and field studies of macroalgae (Leedham et al., 2013).

3.3 Model configuration

The model simulation was run for 3 days from 12:00 UTC 17 November to 12:00 UTC 20 November 2011. We used a nested grid configuration with three grids. The coarsest scale grid covers from 90° E to 135° E and from 14° S to 23° N and uses a spatial resolution of 50 km × 50 km, the next coarsest covers from 106° E to 123° E and from 2° S

to 12° N at a resolution of 10 km × 10 km, and the finest scale grid covers from 112.5° E to 117.25° E and from 3.25° N to 7.75° N and has a spatial resolution of 2 km × 2 km. This horizontal spatial configuration allows the finest grid to completely include the region covered by Flight B on the afternoon of 19 November. The model has 53 vertical levels with varying vertical separation using finer resolution within the boundary layer (50 to 500 m) and between ∼ 13 and 20 km (300 to 500 m) in order to represent accurately the processes in the UTLS (Arteta et al., 2009b). The top of the model reaches to 26.6 km. The model meteorology was initialised and forced along the coarse grid boundaries of C-CATT-BRAMS using 6 hourly European Center for Medium-Range Weather Forecasts (ECMWF) analysis fields for vector wind components, temperature, geopotential height, and specific humidity. We used the ECMWF operational analysis at a 50 km × 50 km resolution. Various chemical species were initialised and forced along the coarse grid boundaries using 6 hourly output from the TOMCAT CTM (Chipperfield, 2006), which were: $CHBr_3$, O_3, hydrogen peroxide, nitrogen oxide, nitrogen dioxide (NO_2), nitric acid, pernitric acid, CO, methane, ethane, propane, isoprene, HCHO, methaldehyde, ethaldehyde, acetone, peroxy actyl nitrate, peroxy propyl nitrate, methyl hydroperoxide, ethyl hydroperoxide, molecular bromine (Br_2), bromine oxide (BrO), hypobromous acid (HOBr), HBr, and $BrONO_2$, bromo carbonyls ($Br_2C(=O)$ and $HBrC(=O)$), and bromo peroxides ($CHBr_2OOH$ and CBr_3COOH). Note that the TOMCAT simulation was run using the same Pyle et al. (2011) emissions. For some of these species we had to perform lumping, splitting, and scaling by reactivity in order to achieve consistency with the chemical mechanism used in CATT-BRAMS. Within the coarsest two model grids we enabled the parameterisations for shallow cumulus convection and for deep convection. We used the deep convection parameterisation from Grell and Dévényi (2002) as implemented in CATT-BRAMS in (Freitas et al., 2009). We allowed the model to resolve clouds and convective processes directly for the finest resolution grid. The topography used in the model has a 10 km resolution within the coarsest two grids and a 1 km resolution within the finest grid. Figure 6 shows a portion

of the topography within the finest model grid. Sea surface temperatures (SSTs) were initialised using the satellite observed weekly average SSTs (Reynolds et al., 2002).

4 Results and discussion

4.1 Meteorological evaluation

In order to support our conclusions regarding the chemistry and transport of $CHBr_3$ within convective clouds, and to properly assess uncertainties within this case study, we need to validate the meteorological simulation and discuss its limitations. To carry out this assessment we have assembled meteorological observations made during the three day simulation.

4.1.1 Radiosonde observations

Radiosondes were launched from Kuching (1°31′ N at 110°20′ E) and the Sonne RV during the three day simulation (Fig. 1). Twenty radiosondes were launched from the Sonne RV during the period of the simulation. The times of launch and the corresponding locations are summarised in Table 3. Comparison between the averaged modelled and observed meteorological variables above Kuching and above the Sonne RV show that the model on average reproduces the observed temperature and wind patterns reasonably well (Figs. 7 and 8). Note that both Kuching and the Sonne RV voyage were within the secondary grid, which used a resolution of 10 km × 10 km. This correspondence between the grid and the observing location and platform hold true for the remaining sections.

4.1.2 Aircraft observations

Observations from Flight A were compared to the model output from the secondary model grid (10 km × 10 km), and the observations from Flight B were compared to the

finest model grid (2 km × 2 km). These comparisons hold for the following sections as well. Figure 9 shows a comparison between the average simulated and observed temperature from both Falcon flights. The model reproduces the vertical temperature profile of Flight A well, but is persistently biased low by up to 2.5 °C. The model temperature shows much better performance during Flight B with no obvious bias, a good vertical profile, and errors of only up to 1.5 °C. Figure 10 indicates that the simulated wind direction compares qualitatively well to observations along both flight tracks reproducing the overall pattern of variability and the mean with one notable exception. During Flight A the model fails to represent the low altitude level wind direction by up to 100° between 12:00 and 13:00 LT. This exception is reflected in the mean wind direction errors for Flights A and B which are 40.3° and 1.7°, respectively. In addition, the model simulates the wind speed qualitatively well capturing the general features. The poorest period of performance occurs in the low altitude portion of Flight A within the boundary layer, mentioned above, between 12:00 and 13:00 LT. The mean model wind speed is biased low during both flights by 0.61 ms^{-1} and 0.58 ms^{-1} for Flights A and B, respectively. In general, the model provides smoother features than observed, which is expected because of its coarser spatial and time resolutions compared to the observations. The errors in the wind direction and speed during the low level portion of Flight A are likely due to unrepresented small scale dynamics within the boundary layer. However, this region remains dynamically unconnected with the region surrounding the Flight B track and therefore these issues will not affect our conclusions regarding the chemistry and transport of $CHBr_3$ during the convective activity near there.

4.1.3 Rainfall observations

Given that rainfall is a proxy for convection, and that rainfall plays a significant role in the washout of PGs it is necessary to establish the performance of the precipitation simulation. Figure 3 compares the radar observed rainfall rates at 2 km to the simulated rainfall rate at the surface and to the simulated precipitation concentration at 2 km throughout Flight B at one hour intervals running from 15:00 to 19:00 LT. The comparison between

the radar rainfall rate and the model is broken into three specific geographical zones: the oceanic, coastal (defined as being either 50 km from the coast over the ocean or between the coast and the peaks of the first inland mountain range as shown in Fig. 6), and the inland zones. We make this distinction based on the relative performance of the model within these zones and also the varying usefulness of the radar data.

The model does not perform well in the oceanic zone. The rainfall close to Region 1 associated with out flowing anvils is not represented in the simulation at the surface appearing only as precipitation in the upper model layers.The spatial extent of the rainfall in the western part of the oceanic zone (running North from 114° E 5.25° N) shown clearly in Figs. 3 and 4 is well represented. However, within this western area, the rainfall is too spatially confined occurring only within overly intense isolated pockets, whereas the observed rainfall pattern is more diffuse and is in general less intense. The temporal evolution of the rainfall is not ideally represented in the model in the western oceanic zone either since the model predicts a small decline in rainfall in this zone during the course of Flight B, but the observations indicate that the rain continues unabated in this part of the oceanic zone. Finally, although not shown, the discrepancy within the simulation in the oceanic zone continues throughout the evening after Flight B. The radar data illustrates that rain associated with convective outflow occurs predominantly over the ocean and a portion of the convection events trigger within the oceanic zone instead of being predominantly within the coastal zone. The model fails to represent either phenomena during most of the evening, but does begin to simulate the triggering of convection over the ocean after a delay of about 6 h.

During Flight B the model in general performs well in the coastal zone capturing the location and onset of the rainfall. Of particular importance is the way in which the model simulates the spatial location of the observed convection upwind of Region 1 at Region 2A during this period shown in Figs. 2, 3c and 4; the model simulates the rainfall close to this region further to the South and East than is observed and more over the land. We term the region that is the genesis of the convection in the model in this area Region 2B (see Figs. 2 and 3c), which is located to the South (by 50 km)

and slightly to the East of Region 2A. In addition to this offset in location, the simulated convective rainfall at Region 2B differs from that observed at Region 2A by the intensity of the rainfall. In the worst case, this is by up to a factor of ~ 5 (100 mm hr^{-1} compared to 20 mm hr^{-1}, see Fig. 3e and f) within the most intense period of rainfall in the simulation, but this only occurs within a limited time period during Flight B. Generally, though, the overestimation is smaller with peak simulated rainfall rates being more comparable to the observed rates (20 mm hr^{-1} compared to 10 mm hr^{-1}). Finally, the model does tend to overestimate the spatial extent of the regions that exhibit the peak rainfall rate. There is also a lack of precipitation from the anvil at the surface even though the model does simulate precipitation at high altitude that does not reach the ground.

In the inland zone, the model simulates a substantial increase of rainfall during the course of Flight B, and this increase is only partially observed by the radar since it only shows a modest increase in extent and intensity. The radar observations in the inland zone are likely occluded by the mountainous areas shown in Fig. 6.

In general, over all three zones, the model over estimates the intensity of the rainfall within the convective columns and shows an apparent lack of surface rainfall associated with the anvil outflow. We did examine the simulated amounts of condensate and precipitation in the upper model levels and their amounts show the presence of anvil outflow and its associated precipitation, but their levels indicate overly intense dehydration.

4.1.4 Discussion of meteorology

We will now discuss how the performance of the meteorological simulation supports our conclusions, how it affects the limitations of our study, and describe how it relates to existing work.

The model simulates the temperature and horizontal winds very well across a range of different locations throughout the entire simulation. In addition, the model adequately simulates the location and onset of the rainfall in the coastal zone including within the important Region 2B thus creating the necessary vertical transport pathway to loft

chemical tracers to higher altitudes. Therefore, from a dynamical standpoint, the simulation forms a sufficient basis for the case study. However, there are three important caveats regarding the performance of the simulated convection and rainfall relative to observations. We will now describe them and the effect they have upon our conclusions. The caveats relate to the location of the convective event during Flight B, the intensity of the rainfall within the convective column, and the model representation of the anvil cloud.

First, Region 2B (simulated) is located ∼ 50 km to the South of Region 2A (observed) and slightly further to the East. This spatial offset between Region 2A and 2B could change the location of the convective cloud in the horizontal plane relative to the $CHBr_3$ distribution and the emissions. This could in turn control the amount of $CHBr_3$ entering the convective column and how much gets lofted to higher altitudes. After accounting for the surface winds that feed into Regions 2A and 2B, the levels of $CHBr_3$ within each region, the different vertical mixing heights in each region, and the amounts present in upwind areas, we find that the $CHBr_3$ levels are substantially similar in both regions: 2.2–3.4 pmol mol^{-1} within Region 2A and ∼ 2–3 pmol mol^{-1} (estimated) within Region 2B. To account for the 50 km of horizontal spatial difference between Region 2A and 2B we apply a 50 km offset (southwards) to the aircraft flight track. After applying this offset, the aircraft track samples the simulated outflow from the convective plume. We also note that Fig. 11 shows that the convective column lofts $CHBr_3$ to up to 12 km and beyond, which is consistent with the altitude at which the Falcon flew during Flight B. This indicates that the vertical transport pathway is qualitatively similar to that which initiates at Region 2A and whose outflow is observed during Flight B.

Regarding the second caveat, the model typically overestimates the rainfall rate within the convective column at Region 2B compared to that observed in Region 2A (by up to a factor of ∼ 5 for the most extreme case, see Fig. 3e and f and discussion in 4.1.3). This discrepancy could affect our conclusions with regard to the washout of soluble species within the convective column. Given this, it is likely that the simulation

gives an upper bound for the washout rate and removal of soluble species within the convective column.

Regarding the third caveat, the lack of simulated rainfall at the surface due to the outflow anvil means that there is almost certainly less precipitation occurring within the anvil since more intense rainfall would not completely evaporate before reaching the surface. As a consequence of this underestimate, less of the soluble species will be washed out in the outflow region. Therefore, this simulation estimates a lower bound for the removal of soluble species by wet deposition within the convection anvil. It is possible that the problems expressed in the latter two caveats cancel one another out to some degree and that they are related: the former causing the latter, since overly intense rainfall within the column itself may lead to increased dehydration in the upper model levels perhaps explaining the lack of surface precipitation associated with convection anvils. The simulated amounts of precipitation within and just below the anvil indicate overly intense dehydration, which is consistent with this explanation. The performance of CATT-BRAMS rainfall simulation described here is consistent with the model's previous performance over this region (Arteta et al., 2009a) where it tended to overestimate the rainfall overland, underestimate rainfall over ocean, overestimate the rainfall rate within the convective column, and underestimate the rainfall in the anvil.

The model captures the general features of the Johnson et al. (2004) conceptual model and its underlying causes during the period of interest: the correct onset of the sea breeze and its location, the consequent convergence inland, and the initiation location of the convection during the morning and afternoon to within an error of 50 km. Most importantly, the model reproduces the Johnson et al. (2004) behaviour reasonably well during the comparison with Flight B. The most significant inconsistency between the simulation and the Johnson et al. (2004) model is the delay in onset of convection initiating over the ocean (∼ 6 h). However, this period of poor performance in the simulation occurs late evening after the comparison with Flight B, and therefore the model's representation of the conceptual model of Johnson et al. (2004) is adequate given the location and time upon which we focus.

4.2 Evaluation of chemistry

Having established that the simulation offers a sufficiently realistic representation of the meteorology during the case study, we now attempt to evaluate the simulation's distribution of $CHBr_3$. We present $CHBr_3$ observations made onboard the Sonne RV, local boats, and the Falcon, and from a ground station at Bukit Atur, Sabah, Malaysia, and compare them to the model simulation. Note that Bukit Atur lies within the secondary model grid, which has a spatial resolution of 10 km × 10 km. In addition to $CHBr_3$ (from the GHOST-MS instrument), we use observations of O_3 (from the UV-O_3 instrument) and CO (from SPIRIT) from the Falcon flights and climatologies of hydroxyl radical (OH) concentrations to further assess the model simulation. Note that from this point onwards the 50 km southward offset is applied to all comparisons and discussions involving Flight B.

Figure 13 shows the simulation results for $CHBr_3$ compared to observations made at various locations. The model tends to overestimate $CHBr_3$. This is particularly the case for background values during Flights A and B (at high altitudes during both flights) and at Bukit Atur (Table 4). Within the instrumental uncertainty the model reasonably reproduces the magnitude of the observed enhancements in $CHBr_3$ due to convective outflow at 12 km during Flight B, which is one focus of the case study. Therefore, our conclusions regarding the chemistry and transport of the VSLS within the convective outflow from Region 2B are well supported, and we infer too that this is also true for the results within the convective column itself. It should be noted that the model simulated other convective events along the northern coast of Borneo, and the peak $CHBr_3$ within the resulting convective outflow plumes tends to be higher than the amount of $CHBr_3$ observed during Flight B by GHOST-MS. For example, Fig. 12 shows another plume at 12 km moving West from 114.5° E and 4° N that contains $CHBr_3$ mixing ratios of up to 1.4 pmol mol^{-1}. Further, examining the plumes originating from convection within Region 2B in more complete fashion reveals that the enhancements in $CHBr_3$ due to convective uplift range from 0.85 to 1.2 pmol mol^{-1}. Thus, the offset flight track does not

sample the largest enhancements simulated by the model. In addition, the background $CHBr_3$ levels at 12 km reach as low as 0.8 pmol mol^{-1} in regions unaffected by recent convective outflow.

The model performs best in comparison with the Sonne RV cruise $CHBr_3$ observations, and, crucially, these observations were made close to the coast where the Pyle et al. (2011) emissions are at their highest. Another small boat transect from Kota Kinabalu to 6°4′ N 115°55′ E (see Fig. 1) was made early on the 23 November LT, and the observed $CHBr_3$ during that trip identified a range of $CHBr_3$ mixing ratios of between 2 pmol mol^{-1} and 3.6 pmol mol^{-1}. The model estimates $CHBr_3$ of between 1.8 and 3.7 pmol mol^{-1} throughout the simulation, and between 2.1 pmol mol^{-1} and 3.3 pmol mol^{-1} on 19 November at the same locations and at the same time of day. Therefore, both the Sonne RV and Kota Kinabalu boat cruise data are supportive of the emissions along the northern coast of Borneo. Indeed, the climatological emission estimates derived from observations (Ziska et al., 2013) in the coastal zone close to the Flight B path are just 10 % lower than the emissions in the 20 km wide coastal band represented in Pyle et al. (2011). Although, it should be noted that the coastal band in Ziska et al. (2013) is considerably wider than 20 km. In addition, the Kota Kinabalu boat transect is very close to Regions 2A and 2B, so this comparison supports our conclusions regarding the convection observed during Flight B.

The model's apparently poor performance in comparison to the observations made at Bukit Atur requires careful qualification since the Pyle et al. (2011) emissions used in this work have been previously validated at this location. $CHBr_3$ has been measured at Bukit Atur since April 2008, and the data show variability in the background throughout the year (Robinson et al., in preparation). Defining the background at the lowest 25 % percentile, these observations indicate that the background is typically lowest during the onset of the monsoons: 0.9 pmol mol^{-1} for the 2009 winter monsoon during November and 0.7 pmol mol^{-1} for the 2009 summer monsoon in June, which are both consistent with the observed values shown in this study (Table 4). They also show that the background tends to be higher at 1.2 pmol mol^{-1} January through May. The Pyle

et al. (2011) emissions used in this study are seasonally invariant and were optimised throughout the year for a mean of 1.3 pmol mol^{-1} at Bukit Atur, which is consistent with the Robinson et al. (2013) data. Thus, the emissions used were adapted for more typical conditions; our simulation compares well to the reported values throughout most of the year and, by this comparison, the emissions perform well. In this context the observed $CHBr_3$ values at the onset of the winter monsoon period during SHIVA are somewhat exceptional. There are two possible causes of the observed lower $CHBr_3$ levels during the winter monsoon onset: seasonal variability in the $CHBr_3$ emissions, and seasonal variability in the dynamics that change the transport pathways between the source regions and Bukit Atur. For the model simulation, this either implies that the Pyle et al. (2011) emissions lack required seasonal variability, or, because the large scale dynamics are well represented in the model, that the emissions are too high in a region dynamically connected to Borneo during the winter monsoon. It is also possible that differences in the representation of boundary layer mixing between the CTM used by Pyle et al., 2011 and CATT-BRAMS could be responsible for the disagreement at Bukit Atur. Finally, the model exhibits various small transient over and underestimations of $CHBr_3$ in the comparisons close to the $CHBr_3$ source regions, and, in the case of the latter, this could be due to unrepresented inhomogeneity in the real emissions (see Fig. 13d). We also note differences in the observed $CHBr_3$ mixing ratios from WASP and GHOST from coincident measurements of both instruments; these two datasets will be examined in further detail in Sala et al. (2013). Note that part of the difference between the observed means during Flight A for both the WASP and GHOST instruments, and between the relevant simulated means and backgrounds, can be explained by the different sampling altitudes of each instrument. WASP was unable to sample at altitudes higher than 6 km, which explains why its observed mean is higher and why the model simulated higher $CHBr_3$ at the points at which it made observations. In summary, despite the identified problems, the comparison to the $CHBr_3$ observations supports our conclusions regarding bromine chemistry within the cloud and outflow argued in the following sections, validates the $CHBr_3$ emissions (Pyle et al.,

2011) throughout most of the year at Bukit Atur, but raises some doubts over the the performance of the emissions during SHIVA at a wide range of locations.

Figure 14 presents a comparison between the simulated and observed O_3 (from the UV-O_3 instrument) and CO (from SPIRIT) along the flight paths of Flight A and Flight B. Figure 14a and c indicates that the model simulates enhanced O_3 and CO during the low altitude portion of Flight A that is associated with urban pollution. However, no evidence of this urban pollution was detected by the aircraft. We speculate that this is either caused by a problem with the simulated boundary layer height, or that the emissions of pollutants is overestimated. Figure 14b shows that elevated levels of CO were observed during a portion of the flight at 12 km that are associated with convective outflow. The model successfully simulates the convective outflow and the magnitude of the enhancements in CO, but the model fails to simulate the background of CO with a high bias of 15 nmol mol^{-1}. This error in the background levels of CO is at least partly due to overestimates of the background in the TOMCAT initial and boundary conditions. However, this will not affect our conclusions regarding bromine chemistry. Figure 14 shows that during Flight B the model underestimates the background O_3 at 12 km by between 5–10 nmol mol^{-1}. This discrepancy could lead to an underestimate of OH production by up to 25 %, which could in turn affect the bromoform lifetime in the model since the reaction between OH and $CHBr_3$ accounts for up to $\sim$ 23 % of the $CHBr_3$ loss term. This is particularly the case near the surface where OH oxidation may compete with the generally faster photolysis sink. We perform a comparison between the model's simulated OH and the various reported climatologies and observations over this region using the same methodology as Marécal et al. (2012). The model simulates very similar vertical profiles (not shown) as reported in Marécal et al., 2012, which were themselves reasonable, and we therefore conclude that the quality of the OH simulation is sufficient (Tan et al., 2001; Spivakovsky et al., 2000).

4.3 Discussion of chemistry

We attempt to estimate both the simulated and observed transport efficiencies from the base of the convective columns to both the point of detrainment and to within the convective outflow. At 14:00 LT, immediately prior to the onset of convective activity, the simulated $CHBr_3$ mixing ratios in the boundary layer, at the base of this convective column in Region 2B effectively range between 2 to 3 pmol mol^{-1}. After the onset of convection at 16:00 LT, the model estimates that at the point of detrainment in the convective column (11 to 12 km) there is up to 1.2 pmol mol^{-1} of $CHBr_3$ (see Figs. 11b and 12a). Mixing ratios at the point of detrainment (11 to 12 km) are therefore between 40 % to 60 % of those near the base of the convective column. In the model, at 18:00, downwind in an area 50 km South of Region 1, and at an altitude of 12 km, $CHBr_3$ mixing ratios are only 33 % to 50 % as large as the boundary mixing ratios in Region 2B. This is because the convective outflow disperses and the modelled $CHBr_3$ mixing ratios drop to a peak of 1.0 pmol mol^{-1} (see Fig. 12c). For the observations, the closest $CHBr_3$ observations to Region 2A at the surface were made during the local boat voyage from Kota Kinabalu that detected between 2 pmol mol^{-1} and 3.6 pmol mol^{-1}. Meanwhile, the GHOST instrument on board the Falcon observed $CHBr_3$ mixing ratios in Region 1 within the convective outflow of up to 0.9 pmol mol^{-1} at an altitude of 12 km (see Fig. 13c), which is equivalent to a relative difference of 25 % to 45 % between the $CHBr_3$ VMRs in the outflow and at the base of the convective column. Therefore, the modelled relative differences for $CHBr_3$ compare very favourably to the observed relative differences. Despite the relatively small geographical offset between Region 2A and 2B, the model simulates that the convective event transports air from the boundary layer to 12 km with a similar efficiency to the observed event. The simulated differences in transport efficiency at varying locations along the outflow plume highlights the need for future aircraft missions to sample vertically within the boundary layer prior to convective activity and along the resulting outflow plume.

We would like to highlight the apparent interaction between the enhanced emissions of $CHBr_3$ near the coast, the diurnal sea breeze, and the resulting convective uplift. Sea breeze driven convection has been shown to be an important cause of convection within the Maritime Continent (Houze et al., 1981; Johnson et al., 1982, 2004; Dudhia, 1989; Wu et al., 2008). Additionally, the local boat cruises during SHIVA, have established that $CHBr_3$ mixing ratios are elevated near the coast, which is indicative of enhanced emissions within these areas. Therefore, we hypothesise that the spatial overlap of high emissions and fast transport pathways to higher altitudes could lead to enhanced transport of SGs and PGs to the stratosphere. It is certainly a currently unexplored source of uncertainty in global models, and is particularly relevant given the remaining uncertainties in the emissions of SGs (Hossaini et al., 2013). This is also highly relevant due to the assumptions used to estimate strat-Br_y^{VSLS} in CTMs and CCMs where a uniform average VSLS mixing ratio is distributed at the surface throughout the tropics (Table 1). Sensitivity studies within global and regional models may be required as part of future work to explore how different configurations of the emission spatial distribution affect transport of SGs and PGs to the stratosphere. Further, such studies need not be limited to exploring convection initiated by sea breeze convergence since large synoptic flow patterns also lead to large scale spatially coherent patterns of convection.

In order to discuss the chemistry and transport of the different PGs we have defined two classifications of PG: inorganic PGs include bromine radicals (Br), molecular bromine (Br_2), bromine oxide (BrO), hypobromous acid (HOBr), hydrobromic acid (HBr), and bromine nitrate ($BrONO_2$); organic PGs include carbonyl bromide $Br_2C(=O)$, formyl bromide HBrC(=O), $CHBr_2OOH$, and CBr_3COOH. Figure 15 provide a summary of the estimated budget of bromine atoms within the modelled convective cloud in Region 2B. These figures estimate the budget of bromine between $CHBr_3$, and inorganic and organic PGs. Figure 15 shows the mixing ratios of bromine atoms split between these three groups of species and the relative contributions each makes to the bromine atom budget. In addition, Table 5 summarises these results and also includes values

from 18:00 LT at 11 to 12 km within Region 1 and from a range of timesteps within background air at 11 to 12 km (not shown in a Figure) indicating how these values change in the convective outflow plume and in high altitude air unaffected by recent convection, respectively. In summary, $CHBr_3$ dominates the bromine atom budget at all locations below 14 km. Of particular importance, $CHBr_3$ dominates the bromine atom budget (70 to 90 %) within the convective column and it therefore plays a key role in the vertical transport of bromine atoms. However, the dominance of $CHBr_3$ diminishes as the outflow plume moves away from the point of detrainment. Conversely, inorganic bromine is vastly reduced within the column and the outflow plume relative to its background in both the free troposphere and at the level of peak detrainment (11 to 12 km) due to washout, inorganic bromine dominates the bromine atom budget above 14 km, and its contribution to the bromine budget in the outflow plume increases with both time and distance from the moment of detrainment. The relative increase and decrease, respectively, of both inorganic PGs and $CHBr_3$ with time within the outflow plume is due to the effect of mixing with background air at 11 to 12 km that is relatively depleted in $CHBr_3$ but enriched in inorganic PGs. In addition, there is reduced washout in the anvil relative to the column and less removal of the inorganic PGs. Overall, this implies that convection has the effect of lofting air to these altitudes that is both depleted in PGs and enriched in $CHBr_3$. It may also be the case that entrainment of background air within the convective column along its length and at the point of detrainment may lead to loss of inorganic PGs due to washout within these air masses too. Thus, overall the convection leads to net vertical transport of bromine, but net loss of PGs at the altitude of detrainment within the short term. Note, above 14 km, the estimated inorganic PG budget (50–60 % of the total budget) is substantially similar to the TOMCAT initial conditions (not shown here). Within the time frame of the C-CATT-BRAMS simulation (3 days), there is little direct transport via convection above 14 km and the other transport pathways are comparatively slow. Thus, the TOMCAT chemistry, transport and removal mechanisms for PGs account for the bulk of the budget in this portion of the atmosphere. In addition, due to the similarity of the Br_y to the initial conditions at 14 km,

we surmise that the lifetimes and removal rates of inorganic PGs are similar within both models. Further, removal rates of Br_y are generally slow within this atmospheric region due to the substantial dehydration that has occurred within air reaching this altitude, which is consistent with the findings of Aschmann et al. (2011). Finally, this is also partially the case for background air at 11 to 12 km that is unaffected by recent convective outflow. However, there is still some moderate influence from the simulated convection within C-CATT-BRAMS that occurs during the course of the simulation causing it to differ from the TOMCAT initial conditions.

Organic PGs only make a small contribution to the total bromine atom budget within the convective cloud and at higher altitudes. Despite this, their mixing ratios are more elevated in the boundary layer and lower troposphere, and, within regions of the atmosphere with near background levels of $CHBr_3$ such as in the free troposphere, where they contribute up to 10 % of the total bromine atoms budget. Their larger relative contribution within the free troposphere indicates that if these air masses could be lofted vertically, these compounds may make a larger relative contribution to the high altitude bromine budget. However, observations of the major organic PGs (CBr_2O and CHBrO) have yet to be made. The absolute values of the organic PG mixing ratios still only peak up to 0.26 pmol mol^{-1} within the boundary layer and free troposphere, however. These findings are consistent with those of Hossaini et al. (2010), which also concluded that the organic PGs could be ignored from chemical mechanisms within CTMs to reduce the future computational burden when estimating strat-Br_y^{VSLS}.

There are two anomalies in the inorganic bromine budget that each occur close to but outside of the convective column. Each has a different cause and will individually require careful explanation. In the first instance, the mixing ratios of the inorganic PGs are elevated in the region to the East of the base of the convective cloud (up to 3.25 pmol mol^{-1}) and in the second case in plumes surrounding the cloud at 3 km (up to 2 pmol mol^{-1}). For the first case, elevated amounts of inorganic bromine (up to 3.25 pmol mol^{-1}) are simulated just outside of the base of the convective cloud and is predominantly composed of HBr, dissolved HBr within cloud particles, HOBr, and Br_2

(listed in order of abundance). The high amounts of inorganic bromine arises due to a similar bromine explosion mechanism as discussed in Marécal et al. (2012) involving (R1), but in this instance the cycle leading to Br_2 production is modified with the presence of urban pollution due to this event's proximity to Kota Kinabalu and the consequently high levels of HCHO simulated by the model (12 nmol mol^{-1}) in the boundary layer. HCHO can react with bromine radicals to produce HBr via (R2). Due to its high abundance, HCHO competes very effectively for the available bromine radicals and leads to excess HBr production, which reduces the production of Br_2 from (R1) by limiting the formation rate of HOBr. The presence of clouds as opposed to rain is key in mediating this process without removing the inorganic bromine. This mechanism could affect the amount of inorganic PG lofted to higher altitude by controlling the relative partitioning between HBr and the Br_x group: BrO, Br_2, and HOBr. On the other hand, the plume of elevated inorganic bromine at 3 km extending between 115.5° E and 116° E is predominantly composed of HBr (0.9 pmol mol^{-1}), HOBr (0.6 pmol mol^{-1}) and $BrONO_2$ (0.45 pmol mol^{-1}). This plume is transported from an area close to Kota Kinabalu via the sea breeze circulation over the course of several hours, it has elevated levels of NO_2 (1.4 nmol mol^{-1}) due to the urban influence, but has slightly lower levels of HCHO (0.5 to 0.8 nmol mol^{-1}) than the previously discussed case primarily due to the HCHO photochemical lifetime (3–4 h). The elevated levels of NO_2 react with BrO present within plume and with background BrO via (R3), which is mixed into the plume in transit, and this leads to modest production of $BrONO_2$. $BrONO_2$ can in turn be photolysed to produce nitrate radicals, which are quickly lost to reform NO_2, and bromine radicals that can react with the available HCHO to produce HBr, or which can react with O_3 to produce BrO. Both of these reaction pathways show similarities to the potential interactions between marine influenced air and urban pollution highlighted in von Glasow et al. (2012).

The relative contribution made by $CHBr_3$ and inorganic and organic PGs within the convective cloud, the free troposphere, and in the outflow region is driven by the varying solubilities of each component of the two types of PGs compared to that of $CHBr_3$.

$CHBr_3$ itself is very insoluble, which explains its relative dominance of the bromine atom budget within the cloud. We classify inorganic and organic PGs into soluble and insoluble forms: insoluble inorganic PGs consist of Br, Br_2, and BrO; soluble inorganic PGs are HOBr, HBr, and $BrONO_2$; the soluble organic PGs are the organic bromo peroxides; and the insoluble organic PGs are the bromo carbonyls. Figures 16 and 17 show very clearly that for the organic PGs the peroxide species are efficiently washed out within the convective column, and the carbonyl species dominate the organic PG contribution within the cloud. The insoluble organic carbonyl PGs also dominate the organic PG contribution to the free tropospheric bromine atom budget. As expected, the soluble inorganic PGs are washed out efficiently within the convective cloud, but they make significant contributions to the bromine atom budget at high altitude > 14 km and in certain areas outside of the cloud at low altitude, which were discussed in detail earlier and explained. The insoluble inorganic PGs are actually present within the cloud below background levels, and this is due to the contribution made by BrO, which is found in higher abundances outside of the cloud where O_3 and Br radical mixing ratios are higher. However, another contributor to insoluble inorganic PGs is Br_2, which is slightly elevated within the convective column compared to air outside the column (see Fig. 18). This is due to the bromine explosion mechanism proposed by Barrie et al. (1988) involving reaction (R1), and discussed in the context of tropical convective clouds by Marécal et al. (2012). Whereby HOBr and HBr react within the aqueous phase to produce Br_2, which is relatively insoluble and is therefore expelled into the gas phase where it can be transported vertically. Br_2 is also elevated around the base of the cloud due to the same mechanism, but there is more Br_2 in this instance because of the elevated levels of HBr and HOBr present there. We should note that there is less Br_2 transported vertically in this simulation than within Marécal et al. (2012) primarily due to the lower amounts of $CHBr_3$ simulated in this study in the coastal marine boundary layer. We can not rule out a larger contribution to the vertical transport of bromine from this mechanism under conditions with higher $CHBr_3$ levels in the marine boundary layer consistent with the observed peaks at other locations. It is also impor-

tant to note the relative contributions of both the inorganic PGs and soluble inorganic PGs within the convective column compared to the free troposphere: inorganic PGs contribute between 25–35 % of the bromine budget in the free troposphere with most of this contribution being due to HBr, but HBr is almost completely absent within the convective column by comparison. The washout of soluble inorganic PGs, and in particular HBr, therefore plays a key role in mediating the transport of bromine atoms to higher altitudes since this process is responsible for removing one of the most abundant components of the lower tropospheric bromine atom budget. Overall, we show a strong dependence between the speciation of inorganic Br_y and its washout rate, and between washout rate and the presence or absence of precipitation. Therefore, inorganic Br_y should be speciated and its washout treated separately for each species within future studies using CTMs and CCMs to estimate strat-Br_y^{VSLS} in order to properly estimate both PG transport within clouds and eventual PGI. In addition, its removal should depend directly upon the presence of precipitation and clouds. This treatment was already implemented within Aschmann et al. (2011) and Hossaini et al. (2012). Liang et al. (2010) modelled the removal of Br_y according to the presence of precipitation and clouds, but did not speciate the Br_y. It is difficult to compare the washout rates within this study to CTMs due to the different spatial and temporal timescales and due to the fact that we analyse a specific convective cloud. However, a removal scheme was implemented within a recent study using a Lagrangian transport model examining individual instances of observed VSLS emissions in the tropical west pacific (Tegtmeier et al., 2012) that allows a comparison. Tegtmeier et al. (2012) estimated that at 12 km up to 65 % of the inorganic PGs was removed that underwent rapid vertical transport due to convection. Within the convection in Region 2B, in this study, we estimate that boundary layer inorganic PG mixing ratios were ~ 4 pmol mol^{-1} prior to the onset of vertical transport, and that they ranged between 0.3 and 0.6 pmol mol^{-1} from 11 to 12 km during the peak of convective activity. Therefore, we estimated a much higher rate of removal (85–92.5 %) compared to Tegtmeier et al. (2012). We qualify this comparison

since we analysed a single instance of convection, and we have identified remaining uncertainties on the rainfall estimates within the convective column within Region 2B.

Given the caveats regarding rainfall intensity and anvil rainfall discussed in Sect. 4.1.4, we still can not eliminate all of the uncertainty regarding the contribution of the soluble bromine species to the Br_y budget at high altitude, nor can we state to what extent the uncertainties in convective column rainfall rate cancel the uncertainties in anvil precipitation. Furthermore, without observations of the inorganic bromine species we have no way to validate the chemistry, transport, and washout of these substances. However, these simulations have allowed for an explicit treatment of the vertical transport of bromine from $CHBr_3$ into the upper tropical tropopause. This has been previously been identified as a significant source of uncertainty (e.g. Law and Sturges, 2007; Montzka and Reiman, 2011), particularly as previous (global) modelling work has generally relied on somewhat crude approximations regarding Br_y and uncertain parameterisations of convection.

5 Conclusions, implications for CTMs and future work

We have presented a successful model simulation of a convective event that occurred along the coast of Borneo due to sea breeze convergence, the consequent transport of $CHBr_3$ to the level of detrainment (11 to 12 km) that was observed, and the chemistry and removal by wet deposition of the $CHBr_3$ PGs within the convective system. Overall, the meteorological simulation was consistent with observations and was sufficient to reproduce the observed transport of SG. However, remaining uncertainties in the rainfall rates within the convective column relative to the convection anvil provide a limitation to our estimates of the washout of soluble PGs. We find that SG transport is the primary process by which bromine is transported up to intermediate high altitudes, i.e. 11 to 12 km, and that this conclusion is well supported by the observations of $CHBr_3$ made during Flight B within the outflow plume and at the surface near to the convective system. Indeed, the model performs very well in simulating the convective

transport pathway from the boundary layer to the outflow region given its strong similarity to the real pathway that was observed. The good performance of the model's simulation of $CHBr_3$ within the outflow plume and the marine boundary layer close to Region 2A is in part due to the usage of the modified emissions of Warwick et al. (2006) developed in Pyle et al. (2011) that were optimised for the Bukit Atur site in Borneo. This good performance was not universal across all of the observing locations, however, since the model had a tendency to overestimate $CHBr_3$ at most other sites. We therefore identified a need to either reassess the seasonal variability of these emissions, or to investigate an overestimate in the emissions within a region dynamically connected to Borneo during the winter monsoon. We found that $CHBr_3$ contributes up to 90 % of the total bromine loading within the convective column and up to 85 % in the convective outflow. Inorganic bromine PGs makes the next largest contribution to the total bromine budget: between 5 to 15 % within the convective column above 4 km, and from 10 to 15 % in the outflow region. The inorganic PGs were depleted in the convective column and the outflow relative to both the background in the free troposphere and at 11 to 12 km. Indeed, the effect of the convective transport at 11 to 12 km was an enhancement of $CHBr_3$, depletion of PGs, but overall net upward transport of bromine. Organic PGs meanwhile provides the smallest contribution, only 3–5 % within the convective column, and up to 5 % in the anvil outflow. Much of these relative contributions is driven by the relative solubility of the PGs to each other and to $CHBr_3$. As expected, soluble species are efficiently removed within the cloud. Outside of the convective system in the free troposphere, soluble inorganic PGs contribute between 25–35 % to the bromine atom budget, but are almost completely removed within the cloud. Therefore the chemical partitioning driven by gas phase chemistry that favours the soluble species (principally HBr) is of key importance. The presence of Br_2 within the convective column, which is insoluble, mitigates the otherwise efficient washout of inorganic PGs within the cloud. Br_2 is formed as a result of aqueous phase chemistry involving HBr and HOBr. However, we did not see evidence of more significant bromine explosion chemistry resulting from reaction (R1) seen in earlier work (Marécal et al.,

2012) that used higher initial concentrations of $CHBr_3$ in the marine boundary layer, but in this study we did not consider the much higher $CHBr_3$ mixing ratios that have been observed in other regions. On the other hand, the main component of the organic PGs are the insoluble species, and therefore, taken as a whole, this class of compounds is less affected by washout.

Using C-CATT_BRAMS Arteta et al. (2009a) demonstrated that different convective parameterisations produce varied estimates of rainfall rate despite reproducing the distribution and onset consistently over SEA-MC, that they tend to overestimate rainfall rates within clouds and underestimate rainfall rates outflow in the anvil, and that there are remaining uncertainties in the associated tracer transport. These uncertainties were not resolved in this study, and the general problem of the rainfall distribution within clouds was reproduced as well, which affects the estimation of soluble PG washout. It is generally known that the performance of convection parameterisations are not consistent across all regions. For example, from this work and from Arteta et al. (2009a) it is evident that the convective rainfall simulation of C-CATT-BRAMS exhibits problems over the SEA-MC. However, it exhibits better performance when predicting rainfall and convection over South America (Freitas et al., 2009) for where it was developed and is well validated. It is therefore possible that CTMs and CCMs using convection parameterisation schemes may also not perform consistently well in every region. This may have the consequence of there being currently unidentified and uncharacterised uncertainties in the estimates of Br_y washout within CTMs and CCMs, which will in turn affect their estimates of PG transport to the UTLS and PGI. At least some of this issue in CATT-BRAMS is linked to the different processes that lead to the initiation of convection; whereas convection is largely driven by thermodynamic instabilities in the atmosphere over South America it is predominantly driven by convergence at varying scales over the SEA-MC. We therefore recommend that there needs to be better validation of the simulated rainfall and tracer transport for all types of deep convective activity in the global chemistry models estimating washout of Br_y across a diverse range of

geographical regions. Further development of modelling capability over this relatively poorly studied region may go some way to resolving these issues.

Through the usage of a combination of the Pyle et al. (2011) emissions and a simulation of convection driven by sea breeze convergence (Johnson et al., 2004), we have demonstrated a synergy between emissions of $CHBr_3$ in coastal regions and a type of convection that initiates close to the coast. Thus, this creates the potential for more direct and enhanced pathways from the $CHBr_3$ source regions in the coastal marine boundary layer to the stratosphere that need to be studied in more detail in future work, and perhaps needs to be considered in global chemistry models. This interaction highlights the potential problem of the assumption of uniform distributions of VSLS within the tropical boundary layer that has been used within various CTM studies (see Table 1).

The minor contribution from organic PGs to Br_y at high altitude implies that they can continue to be ignored in global chemistry models consistent with the conclusions drawn in Hossaini et al. (2010). Although it should be noted that they contributed up to 0.14 pmol mol^{-1} to the high altitude Br_y in our simulation. Inorganic Br_y has been shown to make a non-negligible contribution to the Br_y budget at high altitude, and given the demonstrated importance of the relative solubility of inorganic bromine to its transport efficiency within the convective cloud, we recommend that parameterisations considering its washout should be adopted into CTMs and CCMs. Although we only showed a minor contribution of Br_2 to the Br_y budget at higher altitudes, we can not rule out more significant contributions under different conditions. For example, Marécal et al. (2012) demonstrated that under conditions with the highest plausible $CHBr_3$ mixing ratios Br_2 made a non negligible contribution to the Br_y budget within the cloud and at higher altitude. This is expected due to the non linear scaling in the production of Br_2 due to the second order reaction that leads to its production within cloud droplets. Observations of $CHBr_3$ have revealed that surface mixing ratios can peak at up to 10 to 40 pmol mol^{-1} (Robinson et al., 2013) in along the North East coast of Borneo in Tawau. Therefore, a significant contribution of Br_2 to the Br_y budget within clouds and

at high altitude can not be ruled out and this chemistry may be relevant within the SEA-MC.

We showed that there could potentially be chemical interactions between inorganic bromine resulting from the oxidation of $CHBr_3$ and urban pollution consistent with the proposals of von Glasow et al. (2012). Our case study was focused on the coastal and marine environment close Kota Kinabalu, which is a city populated with over 300 000 people. Consequently, the model simulated elevated levels of NO_x and HCHO derived from the oxidation of volatile organic compounds in this area in combination with elevated levels of inorganic bromine resulting from VSLS oxidation. Under these conditions, we showed that there could be two possible interactions: first, the reaction of bromine radicals with elevated amounts of HCHO via (R2) could lead to elevated HBr, which may disrupt the onset of bromine explosion chemistry involving (R1) near the convective cloud base; second, elevated levels of NO_x were shown to lead to increased $BrONO_2$ production due to the reaction between NO_2 and BrO via (R3). Further research, both through models and observations, is required to understand if these processes are significant in determining the transport of VSLS and PGs to higher altitude or whether they play a role in tropospheric chemistry.

Although the simulation of $CHBr_3$ within the convective system has been well validated and conclusions regarding its transport and chemical loss are well supported, there are, as yet, no observations of inorganic bromine species within the outflow region of tropical convective clouds. Such observations are urgently needed to validate these simulations and to support future work.

Supplementary material related to this article is available online at: http://www.atmos-chem-phys-discuss.net/13/20611/2013/ acpd-13-20611-2013-supplement.pdf.

Acknowledgements. This research has been financially supported through the SHIVA (226224-FP7-ENV-2008-1) project from the European Commission. We are grateful to the

support given by the National Oceanography Directorate (NOD) and the Economic Planning Unit (EPU) of Malaysia. In particular, we are grateful for the support given by Nor Aieni Binti Haji Mokhtar (NOD) and Mrs. Munirah Abd Manan (EPU) without which the SHIVA campaign in the Western Pacific would not have been possible. EA thanks X. Zhu and L. Pope for technical contributions to the canister sample analysis, which was supported from NASA Upper Atmosphere Research Program grants. We thank the Sonne and Falcon teams for their contributions to the SHIVA campaign. CATT-BRAMS is a free software provided by CPTEC/INPE and distributed under the CC-GNU-GPL license.

The publication of this article is financed by CNRS-INSU.

References

Arteta, J., Marécal, V., and Rivière, E. D.: Regional modelling of tracer transport by tropical convection – Part 1: Sensitivity to convection parameterization, Atmos. Chem. Phys., 9, 7081–7100, doi:10.5194/acp-9-7081-2009, 2009a.

Arteta, J., Marécal, V., and Rivière, E. D.: Regional modelling of tracer transport by tropical convection – Part 2: Sensitivity to model resolutions, Atmos. Chem. Phys., 9, 7101–7114, doi:10.5194/acp-9-7101-2009, 2009b.

Arakawa, A. and Schubert, W. H.: Interaction of a cumulus cloud ensemble with the large-scale environment, Part I., J. Atmos. Sci., 31, 674–701, 1974.

Aschmann, J., Sinnhuber, B.-M., Atlas, E. L., and Schauffler, S. M.: Modeling the transport of very short-lived substances into the tropical upper troposphere and lower stratosphere, Atmos. Chem. Phys., 9, 9237–9247, doi:10.5194/acp-9-9237-2009, 2009.

Aschmann, J., Sinnhuber, B.-M., Chipperfield, M. P., and Hossaini, R.: Impact of deep convection and dehydration on bromine loading in the upper troposphere and lower stratosphere, Atmos. Chem. Phys., 11, 2671–2687, doi:10.5194/acp-11-2671-2011, 2011.

Barrie, L. A., Bottenheim, J. W., Schnell, R. C., Crutzen, P. J., and Rasmussen, R. A.: Ozone destruction and photochemical reactions at polar sunrise in the lower arctic atmosphere, Nature, 334, 138–141, 1988.

Chipperfield, M.: New version of the TOMCAT/SLIMCAT offline chemical transport model: intercomparison of stratospheric tracer experiments, Q. J. Roy. Meteor. Soc., 132, 1179–1203, doi:10.1256/qj.05.51, 2006.

Choi, S., Wang, Y., Salawitch, R. J., Canty, T., Joiner, J., Zeng, T., Kurosu, T. P., Chance, K., Richter, A., Huey, L. G., Liao, J., Neuman, J. A., Nowak, J. B., Dibb, J. E., Weinheimer, A. J., Diskin, G., Ryerson, T. B., da Silva, A., Curry, J., Kinnison, D., Tilmes, S., and Levelt, P. F.: Analysis of satellite-derived Arctic tropospheric BrO columns in conjunction with aircraft measurements during ARCTAS and ARCPAC, Atmos. Chem. Phys., 12, 1255–1285, doi:10.5194/acp-12-1255-2012, 2012.

Crassier, V., Suhre, K., Tulet, P., and Rosset, R.: Development of a reduced chemical scheme for use in mesoscale meteorological models, Atmos. Environ., 34, 2633–2644, 2000.

Dorf, M., Butler, J. H., Butz, A., Camy-Peyret, C., Chipperfield, M. P., Kritten, L., Montzka, S. A., Simmes, B., Weidner, F., and Pfeilsticker, K.: Long-term observations of stratospheric bromine reveal slow down in growth, Geophys. Res. Lett., 33, L24803, doi:10.1029/2006GL027714, 2006.

Dudhia, J.: Numerical study of convection observed during the Winter Monsoon Experiment using a mesoscale two-dimensional model, J. Atmos. Sci., 46, 3077–3107, 1989.

Dvortsov, V. L., Geller, M. A., Solomon, S., Schauffler, S. M., Atlas, E. L., and Blake, D. R.: Rethinking reactive halogen budgets in the midlatitude lower stratosphere, Geophys. Res. Lett., 26, 1699–1702, doi:10.1029/1999GL900309, 1999.

Frank, W. M. and Cohen, C.: Simulation of tropical convective systems, Part 1: a cumulus parameterization, J. Atmos. Sci., 44, 3787–3799, 1987.

Freitas, S. R., Longo, K. M., Silva Dias, M. A. F., Chatfield, R., Silva Dias, P., Artaxo, P., Andreae, M. O., Grell, G., Rodrigues, L. F., Fazenda, A., and Panetta, J.: The Coupled Aerosol and Tracer Transport model to the Brazilian developments on the Regional Atmospheric Modeling System (CATT-BRAMS) – Part 1: Model description and evaluation, Atmos. Chem. Phys., 9, 2843–2861, doi:10.5194/acp-9-2843-2009, 2009.

Fueglistaler, S., Dessler, A. E., Dunkerton, T. J., Folkins, I., Fu, Q., and Mote, P. W.: Tropical tropopause layer, Rev. Geophys., 47, RG1004, doi:10.1029/2008RG000267, 2009.

Gettelman, A., Lauritzen, P. H., Park, M., and Kay, J. E.: Processes regulating short-lived species in the tropical tropopause layer, J. Geophys. Res.-Atmos., 114, 4080, doi:10.1029/2009JD011785, 2009.
Grell, G. A.: Prognostic evaluation of assumptions used by cumulus parameterizations, Mon. Weather Rev., 121, 764–787, 1993.
Grell, G. A. and Dévényi, D.: A generalized approach to parameterizing convection combining ensemble and data assimilation, Geophys. Res. Lett., 29, 1693, doi:10.1029/2002GL015311, 2002.
Guimbaud, C., Catoire, V., Gogo, S., Robert, C., Chartier, M., Laggoun-Défarge, F., Grosse, A., Albéric, P., Pomathiod, L., Nicoullaud, B., and Richard, G.: A portable infrared laser spectrometer for flux measurements of trace gases at the geosphere–atmosphere interface, Measurment Science and Technology, 22, 075601, doi:10.1088/0957-0233/22/7/075601, 2011.
Hossaini, R., Chipperfield, M. P., Monge-Sanz, B. M., Richards, N. A. D., Atlas, E., and Blake, D. R.: Bromoform and dibromomethane in the tropics: a 3-D model study of chemistry and transport, Atmos. Chem. Phys., 10, 719–735, doi:10.5194/acp-10-719-2010, 2010.
Hossaini, R., Chipperfield, M. P., Feng, W., Breider, T. J., Atlas, E., Montzka, S. A., Miller, B. R., Moore, F., and Elkins, J.: The contribution of natural and anthropogenic very short-lived species to stratospheric bromine, Atmos. Chem. Phys., 12, 371–380, doi:10.5194/acp-12-371-2012, 2012.
Hossaini, R., Mantle, H., Chipperfield, M. P., Montzka, S. A., Hamer, P., Ziska, F., Quack, B., Krüger, K., Tegtmeier, S., Atlas, E., Sala, S., Engel, A., Bönisch, H., Keber, T., Oram, D., Mills, G., Ordóñez, C., Saiz-Lopez, A., Warwick, N., Liang, Q., Feng, W., Moore, F., Miller, B. R., Marécal, V., Richards, N. A. D., Dorf, M., and Pfeilsticker, K.: Evaluating global emission inventories of biogenic bromocarbons, Atmos. Chem. Phys. Discuss., 13, 12485–12539, doi:10.5194/acpd-13-12485-2013, 2013.
Houze, R., Geotis, S. G., Marks, F. D. Jr., and West, A. K.: Winter Monsoon convection in the vicinity of north Borneo, Part 1: structure and time variation of the clouds and precipitation, Mon. Weather Rev., 109, 1595–1614, 1981.
Johnson, R. H. and Kriete, D. C.: Thermodynamic and circulation characteristics of Winter Monsoon tropical mesoscale convection, Mon. Weather Rev., 110, 1898–1911, 1982.
Johnson, R. H., Aves, S. L., Nesbitt, S. W., and Ciesielski, P. E.: The Diurnal Cycle of Precipitation over the Northern South China Sea, The 2nd TRMM International Science Conference, Nara, Japan, 6 September 2004.

Kain, J. S. and Fritsch, J. M.: Convective Parameterization for Mesoscale Models: The Kain–Fritsch Scheme, the Representation of Cumulus Convection in Numerical Models, edited by: Emmanuel, K. and Raymond, D. J., Am. Meteorol. Soc., Boston, Mass., USA, 246 pp., 1993.
Kerkweg, A., Jöckel, P., Warwick, N., Gebhardt, S., Brenninkmeijer, C. A. M., and Lelieveld, J.: Consistent simulation of bromine chemistry from the marine boundary layer to the stratosphere – Part 2: Bromocarbons, Atmos. Chem. Phys., 8, 5919–5939, doi:10.5194/acp-8-5919-2008, 2008.
Kreycy, S., Camy-Peyret, C., Chipperfield, M. P., Dorf, M., Feng, W., Hossaini, R., Kritten, L., Werner, B., and Pfeilsticker, K.: Atmospheric test of the $J(BrONO_2)/k_{BrO+NO_2}$ ratio: implications for total stratospheric Br_y and bromine-mediated ozone loss, Atmos. Chem. Phys. Discuss., 12, 27821–27845, doi:10.5194/acpd-12-27821-2012, 2012.
Krishnamurti, T. N., Low-Nam, S., and Pash, R.: Cumulus parameterizations and rainfall rates, Mon. Weather Rev., 111, 815–828, 1983.
Krüger, K., Tegtmeier, S., and Rex, M.: Variability of residence time in the Tropical Tropopause Layer during Northern Hemisphere winter, Atmos. Chem. Phys., 9, 6717–6725, doi:10.5194/acp-9-6717-2009, 2009.
Krysztofiak, G., Catoire, V., Poulet, G., Marécal, V., Pirre, M., Louis, F., Canneaux, S., and Josse, B.: Detailed modeling of the atmospheric degradation mechanism of very short-lived brominated species, Atmos. Environ., 59, 514–532, 2012.
Kuo, H. L.: Further studies of the parameterization of the effect of cumulus convection on large-scale flow, J. Atmos. Sci., 31, 1232–1240, 1974.
Law, K. S. and Sturges, W. T.: Halogenated very short-lived substances, in: Scientific Assessment of Ozone Depletion: 2006, Global Ozone Research and Monitoring Project, Report No. 50, Chapt. 2, edited by: World Meteorological Organization, Geneva, 2007.
Leedham, E. C., Hughes, C., Keng, F. S. L., Phang, S.-M., Malin, G., and Sturges, W. T.: Emission of atmospherically significant halocarbons by naturally occurring and farmed tropical macroalgae, Biogeosciences, 10, 3615–3633, doi:10.5194/bg-10-3615-2013, 2013.
Liang, Q., Stolarski, R. S., Kawa, S. R., Nielsen, J. E., Douglass, A. R., Rodriguez, J. M., Blake, D. R., Atlas, E. L., and Ott, L. E.: Finding the missing stratospheric Br_y: a global modeling study of $CHBr_3$ and CH_2Br_2, Atmos. Chem. Phys., 10, 2269–2286, doi:10.5194/acp-10-2269-2010, 2010.
Liu, C. and Zisper, E. J.: Global distribution of convection penetrating the tropical tropopause, J. Geophys. Res.-Atmos., 110, D23104, doi:10.1029/2005JD006063, 2005.

Longo, K. M., Freitas, S. R., Pirre, M., Marécal, V., Rodrigues, L. F., Panetta, J., Alonso, M. F., Rosário, N. E., Moreira, D. S., Gácita, M. S., Arteta, J., Fonseca, R., Stockler, R., Katsurayama, D. M., Fazenda, A., and Bela, M.: The chemistry CATT–BRAMS model (CCATT–BRAMS 4.5): a regional atmospheric model system for integrated air quality and weather forecasting and research, Geosci. Model Dev. Discuss., 6, 1173–1222, doi:10.5194/gmdd-6-1173-2013, 2013.

Marécal, V., Pirre, M., Krysztofiak, G., Hamer, P. D., and Josse, B.: What do we learn about bromoform transport and chemistry in deep convection from fine scale modelling?, Atmos. Chem. Phys., 12, 6073–6093, doi:10.5194/acp-12-6073-2012, 2012.

McLinden, C. A., Haley, C. S., Lloyd, N. D., Hendrick, F., Rozanov, A., Sinnhuber, B.-M., Goutail, F., Degenstein, D. A., Llewellyn, E. J., Sioris, C. E., Van Rozendael, M., Pommereau, J. P., Lotz, W., and Burrows, J. P.: Odin/OSIRIS observations of stratospheric BrO: retrieval methodology, climatology, and inferred Bry, J. Geophys. Res.-Atmos., 115, D15308, doi:10.1029/2009JD012488, 2010.

Mellor, G. and Yamada, T.: Development of a turbulence closure model for geophysical fluid problems, Rev. Geophys., 20, 851–875, 1982.

Montzka, S. A. and Reimann, S.: Ozone-depleting substances (ODSs) and related chemicals, in: Scientific Assessment of Ozone Depletion: 2010, Global Ozone Research and Monitoring Project, Report No. 52, Chapt. 1, edited by: World Meteorological Organization, Geneva, Switzerland, 2011.

Neale, R. and Slingo, J.: The maritime continent and its role in the global climate: a GCM study, J. Climate, 16, 834–848, 2003.

Ordóñez, C., Lamarque, J.-F., Tilmes, S., Kinnison, D. E., Atlas, E. L., Blake, D. R., Sousa Santos, G., Brasseur, G., and Saiz-Lopez, A.: Bromine and iodine chemistry in a global chemistry-climate model: description and evaluation of very short-lived oceanic sources, Atmos. Chem. Phys., 12, 1423–1447, doi:10.5194/acp-12-1423-2012, 2012.

Pfeilsticker, K. and the SHIVA consortium: Overview on the project SHIVA (stratospheric ozone: halogen impacts in a varying atmosphere): achievements and key results, in preparation, 2013.

Pyle, J. A., Ashfold, M. J., Harris, N. R. P., Robinson, A. D., Warwick, N. J., Carver, G. D., Gostlow, B., O'Brien, L. M., Manning, A. J., Phang, S. M., Yong, S. E., Leong, K. P., Ung, E. H., and Ong, S.: Bromoform in the tropical boundary layer of the Maritime Continent during OP3, Atmos. Chem. Phys., 11, 529–542, doi:10.5194/acp-11-529-2011, 2011.

Reynolds, R. W., Rayner, N. A., Smith, T. M., Stokes, D. C., and Wang, W.: An improved in situ and satellite SST analysis for climate, J. Climate, 15, 1609–1625, 2002.

Sioris, C. E., Kovalenko, L. J., McLinden, C. A., Salawitch, R. J., Van Roozendael, M., Goutail, F., Dorf, M., Pfeilsticker, K., Chance, K., von Savigny, C., Liu, X., Kurosu, T. P., Pommereau, J.-P., Boesch, H., and Frerick, J.: Latitudinal and vertical distribution of bromine monoxide in the lower stratosphere from scanning imaging absorption spectrometer for atmospheric chartography limb scattering measurements, J. Geophys. Res.-Atmos., 111, D14301, doi:10.1029/2005JD006479, 2006.

Sinnhuber, B.-M., Rozanov, A., Sheode, N., Afe, O. T., Richter, A., Sinnhuber, M., Wittrock, F., Burrows, J. P., Stiller, G. P., von Clarmann, T., and Linden, A.: Global observations of stratospheric bromine monoxide from SCIAMACHY, Geophys. Res. Lett., 32, L20810, doi:10.1029/2005GL023839, 2005.

Schofield, R., Fueglistaler, S., Wohltmann, I., and Rex, M.: Sensitivity of stratospheric Br_y to uncertainties in very short lived substance emissions and atmospheric transport, Atmos. Chem. Phys., 11, 1379–1392, doi:10.5194/acp-11-1379-2011, 2011.

Spivakovsky, C. M., Logan, J. A. Montzka, S. A., Balkanski, Y. J., Foreman-Fowler, M., Jones, D. B. A., Horowitz, L. W., Fusco, A. C., Brenninkmeijer, C. A. M., Prather, M. J., Wofsy, S. C., and McElroy, M. B.: Three-dimensional climatological distribution of troposheric OH: update and evaluation, J. Geophys. Res., 105, D7, doi:10.1029/1999JD901006, 2000.

Stockwell, W. R., Kirchner, F., Kuhn, M., and Seefeld, S.: A new mechanism for regional atmospheric chemistry modeling, J. Geophys. Res., 102, 25847–25879, 1997.

Tan, D., Faloona, I., Simpas, J. B., Brune, W., Olson, J., Crawford, J., Avery, M., Sachse, G., Vay, S., Sandholm, S., Guan, H.-W., Vaughn, T., Mastromarino, J., Heikes, B., Snow, J., Podolske, J., and Singh, H.: OH and HO_2 in the tropical Pacific: results from PEM-Tropics B, J. Geophys. Res., 106, D23, doi:10.1029/2001JD900002, 2001.

Tegtmeier, S., Krüger, K., Quack, B., Atlas, E. L., Pisso, I., Stohl, A., and Yang, X.: Emission and transport of bromocarbons: from the West Pacific ocean into the stratosphere, Atmos. Chem. Phys., 12, 10633–10648, doi:10.5194/acp-12-10633-2012, 2012.

Toon, O. B., McKay, C. P., Ackerman, T. P., and Santhanan, K. L.: Rapid calculation of radiative heating rates and photodissociation rates in inhomogeneous multiple scattering atmospheres, J. Geophys. Res., 94, 16287–16301, 1989.

Tripoli, G. and Cotton, W.: The Colorado State University three-dimensional cloud-mesoscale model, Part I: general theoretical framework and sensitivity experiments, J. Res. Atmos., 16, 185–219, 1982.

Quack, B. and Wallace, D.: Air-sea flux of bromoform: controls, rates, and implications, Global Biogeochem. Cy., 17, 1023, doi:10.1029/2002GB001890, 2003.

Walko, R. L., Cotton, W. R., Meyers, M. P., and Harrington, J. Y.: New RAMS cloud microphysics parameterization, Part I: the single-moment scheme, Atmos. Res., 38, 29–62, 1995.

Walko, R., Band, L., Baron, J., Kittel, F., Lammers, R., Lee, T., Ojima, D., Pielke, R., Taylor, C., Tague, C., Tremback, C., and Vidale, P.: Coupled atmosphere-biophysics-hydrology models for environmental modeling, J. Appl. Meteorol., 39, 931–944, 2000.

Warwick, N. J., Pyle, J. A., Carver, G. D., Yang, X., Savage, N. H., O'Connor, F. M., and Cox, R. A.: Global modeling of biogenic bromocarbons, J. Geophys. Res.-Atmos., 111, D24305, doi:10.1029/2006JD007264, 2006.

Wu, P. and Yamanaka, M. D.: The formation of nocturnal rainfall offshore from convection over western Kalimantan (Borneo) Island, J. Meteorol. Soc. Jpn., 86, 187–203, 2008.

Ziska, F., Quack, B., Abrahamsson, K., Archer, S. D., Atlas, E., Bell, T., Butler, J. H., Carpenter, L. J., Jones, C. E., Harris, N. R. P., Hepach, H., Heumann, K. G., Hughes, C., Kuss, J., Krüger, K., Liss, P., Moore, R. M., Orlikowska, A., Raimund, S., Reeves, C. E., Reifenhäuser, W., Robinson, A. D., Schall, C., Tanhua, T., Tegtmeier, S., Turner, S., Wang, L., Wallace, D., Williams, J., Yamamoto, H., Yvon-Lewis, S., and Yokouchi, Y.: Global sea-to-air flux climatology for bromoform, dibromomethane and methyl iodide, Atmos. Chem. Phys. Discuss., 13, 5601–5648, doi:10.5194/acpd-13-5601-2013, 2013.

Table 1. A summary of VSLS considered in 3-D global modelling studies that estimate strat-Br_y^{VSLS} and the assumptions used. In the studies that assumed constant boundary layer (BL) and free tropospheric VSLS VMR (volume mixing ratio) the values of 1.6 and 1 pmol mol^{-1} were used for bromoform ($CHBr_3$) and dibromomethane (CH_2Br_2), respectively. Br_y lifetime was assumed to be ~ 10 days in the studies with a constant Br_y lifetime.

Study	VSLS	VSLS source mechanism	Br_y removal	strat-Br_y^{VSLS} contribution
Warwick et al., 2006	$CHBr_3$, CH_2Br_2, and chlorobromocarbons	Top-down estimate within study	Constant lifetime (10 days)	6–7 pmol mol^{-1}
Hossaini et al., 2010	$CHBr_3$, CH_2Br_2	Constant BL VMR (1.2 pmol mol^{-1} for both VSLS)	Constant lifetime (10 days)	2.4 pmol mol^{-1}
Aschmann et al., 2009	$CHBr_3$	Constant BL VMR	Two extremal cases: either Bry experiences no washout or is completely removed by dehydration	1.6–3 pmol mol^{+}
Aschmann et al., 2010	$CHBr_3$, CH_2Br_2 $CHBr_3$, CH_2Br_2 chlorobromocarbons, and halons	Constant BL VMR	Washout dependent on Br_y solubility (two classes of solubility) and simulated moisture	3.4–5 pmol mol^{-1} 4.9–5 pmol mol^{+}
Liang et al., 2010	$CHBr_3$, CH_2Br_2	Top-down estimate	Washout modelled for a single Br_y species according to solubility and rainfall	~ 5 pmol mol^{-1}
Hossaini et al., 2012	$CHBr_3$, CH_2Br_2 $CHBr_3$, CH_2Br_2, chlorobromocarbons, and halons	Constant BL VMR (1 and 1.2 pmol mol^{-1} for both VSLS in different cases)	Washout estimated from prescribed soluble : insoluble Br_y and linked to convective precipitation	~ 4 pmol mol^{-1} 4.9–5.2 pmol mol^{-1}

Table 2. A summary of the all of the observations used according to platform and observing location and, where appropriate, the instrument used.

Platform/Observing Location		Observed Variables
Sonne RV radiosondes		Temperature, wind velocity, wind direction
Kuching radiosondes		Temperature, wind velocity, wind direction
DLR Falcon	Flight A	Temperature, wind velocity, wind direction, SPIRIT CO, UV-O_3 O_3, and WASP GC-MS and GHOST GC-MS $CHBr_3$
	Flight B	Temperature, wind velocity, wind direction, SPIRIT CO, UV-O_3 O_3, and GHOST GC-MS $CHBr_3$
Bukit Atur		$CHBr_3$
Sonne RV cruise		GC-MS $CHBr_3$
Local boat cruise (Kuching)		WASP GC-MS $CHBr_3$
Kota Kinabalu		Rainfall observations from meteorological radar

Table 3. Summary of sonde launches from the Sonne RV. The listed numbered locations correspond to the locations shown in Fig. 1. All times shown in UTC.

Location	Time Range of Launch(es)	Number of Radiosondes Launched
1	17 Nov, 12:00	1
2	17 Nov, 18:00	1
3	18 Nov, 00:00	1
4	18 Nov, 03:00 to 18 Nov, 05:00	2
5	18 Nov, 08:00 to 19 Nov, 00:00	9
6	19 Nov, 02:00	1
7	19 Nov, 04:00	1
8	19 Nov, 12:00	1
9	19 Nov, 18:00	1
10	20 Nov, 00:00	1

Table 4. The observed mean and background $CHBr_3$ mixing ratios from various platforms and instruments summarised from Fig. 13. The simulated mean and backgrounds at the location and time of observation from the various platforms and instruments. All values are in pmol mol^{-1}. The bracketed values for Bukit Atur indicate what they typically observe between January and May.

Platform/Instrument	Model		Observations	
	Mean	Background	Mean	Background
Flight A – GHOST	1.5	1.0	0.7	0.6
Flight A – WASP	2.1	1.3	1.2	0.6
Flight B – GHOST only	0.9	0.8	0.5	0.4
Sonne RV	1.8	1.1	1.6	1.2
Local boat	2.2	2.0	1.5	1.3
Bukit Atur	1.3	1.2	0.9 (1.3)	0.8 (1.2)

Table 5. Simulated mixing ratios of bromine compounds at various altitudes within and outside of the convective cloud. The relative simulated contributions to the total bromine budget from each component are shown in brackets.

Height and location (km)	$CHBr_3$ (pmol mol^{-1})	Inorganic PGs (pmol mol^{-1})	Organic PGs (pmol mol^{-1})	Total bromine (pmol mol^{-1})
0–4 km within convective column cloud	3.75–4.75 (70–90 %)	0.2–1.2 (< 5–20 %)	0.16–0.2 (3–3.5 %)	5–6.5
4–11 km within convective column cloud	2.75–4.25 (80–90 %)	0.2–0.6 (< 5–15 %)	0.15 (3.5–4 %)	3.5–5
11–12 within the convective column cloud	3.25–4 (80–90 %)	0.2–0.6 (5–15 %)	0.14 (3.5 %)	3.9–4.2
Background at 11–12 in absence of clouds and outflow (not shown in Fig. 15)	~ 2.5 (65 %)	~ 1.2 (31 %)	~ 0.15 (4 %)	~ 3.85
11–12 outside convective column but in outflow (not shown in Fig. 15)	3–3.5 (80–85 %)	0.4–0.5 (10–15 %)	~ 0.15 (3.5–4 %)	~ 4
> 14 outside cloud	1.75–2 (35–50 %)	2–2.6 (50–60 %)	0.08–0.1 (1.5–2.5 %)	3.75–4

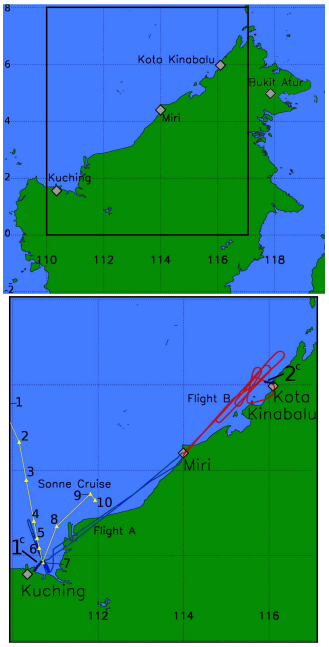

Fig. 1. Overview of Falcon flights from Miri on 19 November (shown in red and blue), of the Sonne RV voyage track between 12:00 UTC 17 November and 00:00 UTC 20 November (shown in yellow), and the local boat voyages from Kuching and Kota Kinabalu. The local boat voyage on 19th coinciding with Flight A and the Sonne RV is labelled 1^c, and the local boat voyage on the 24 November is labelled 2^c. The different launch locations along the Sonne RV voyage track are marked with yellow triangles and numbered according to the numbering scheme shown in Table 3. The ground monitoring station at Bukit Atur is also shown.

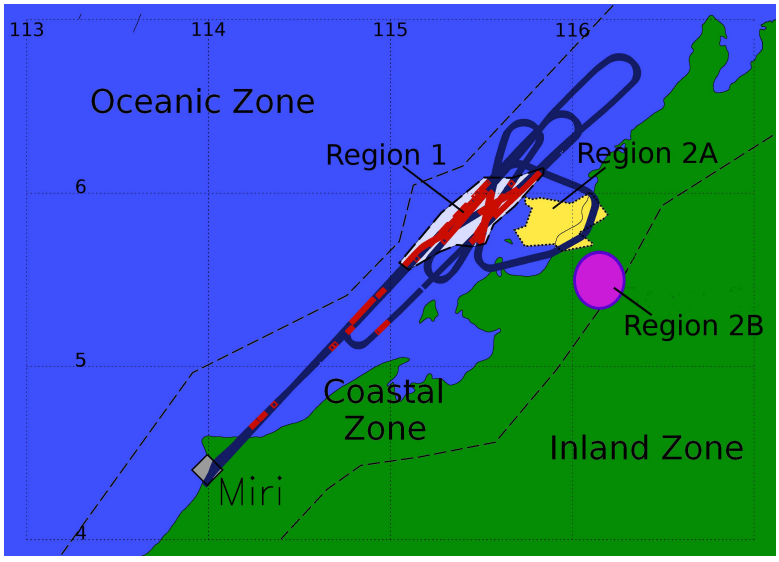

Fig. 2. Overview of convective signatures (red diamonds) observed during Flight B on 19 November. The red diamonds indicate cases where the SPIRIT instrument observed elevated CO (> 80 nmol mol^{-1}) relative to the background at 12 km (~70 nmol mol^{-1}), which captures the convective signatures but excludes the cases where the aircraft flew at low altitude. The area where convective signatures were observed is called Region 1 (very pale blue area). Region 2A (yellow area) and 2B (purple area) are the convective source regions for the outflow observed at Region 1 in the radar observations and in the model, respectively. The Oceanic, Coastal, and Inland Zones are also delineated.

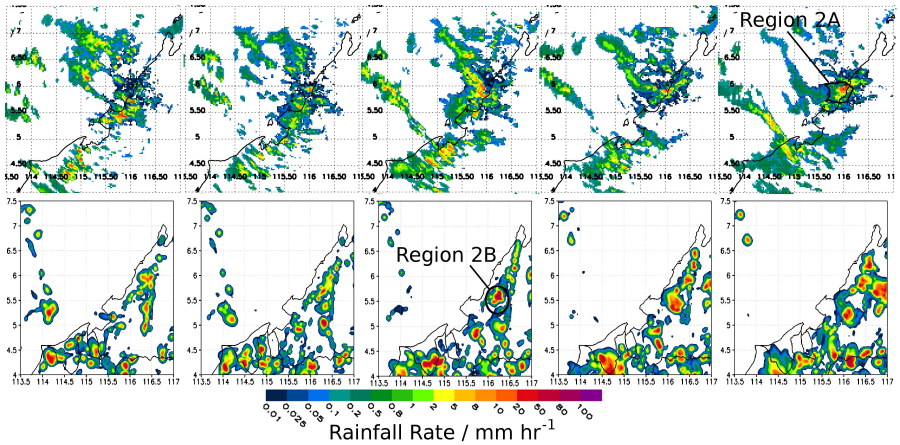

Fig. 3. A comparison between the radar observed rainfall rate at 2 km on the left with the estimated model surface rainfall rate during the course of Flight B from 19 November. The panels from top to bottom represent output and observations of hourly intervals from 15:00 to 19:00. The locations of Regions 2A and 2B are also shown.

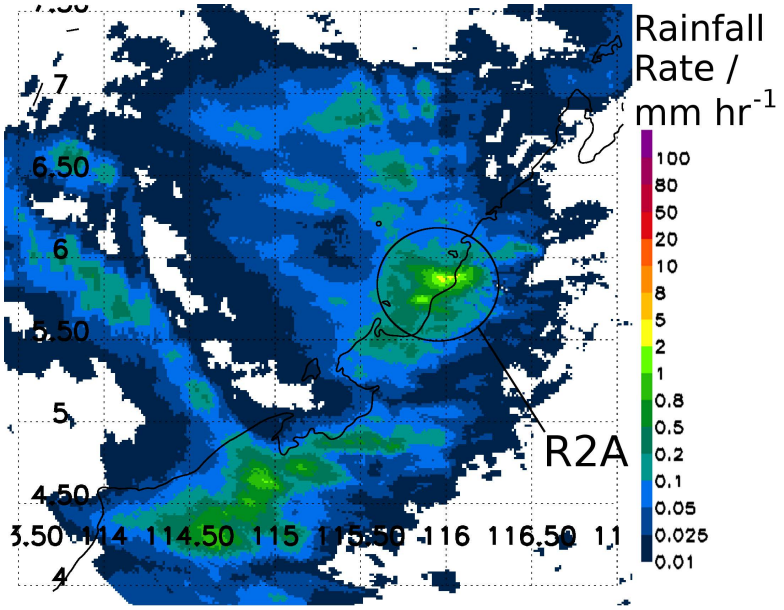

Fig. 4. Average observed radar rainfall rate along the western coast of Borneo centred over Flight B on 19 November. The plot is the temporal average between 14:00 and 19:00. Note the location of Region 2A indicating a center of convective activity.

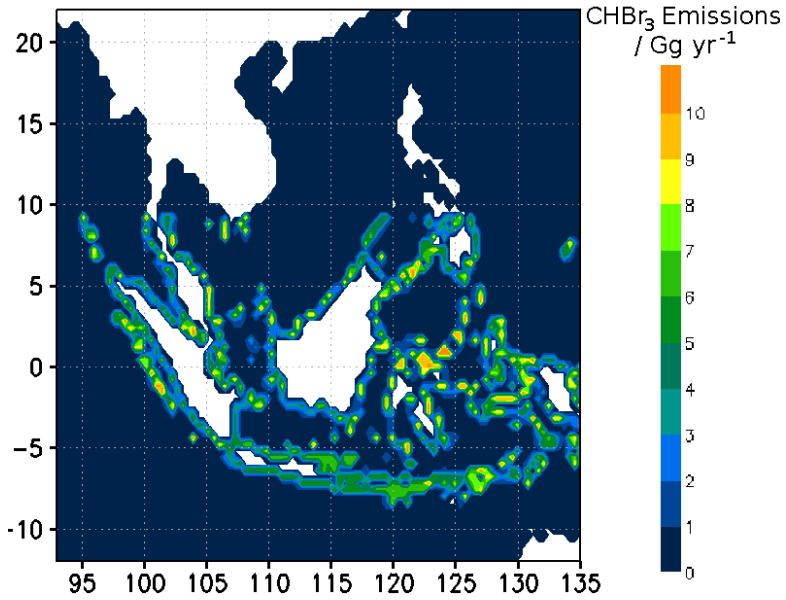

Fig. 5. Map of the annual $CHBr_3$ emission distribution used in CCATT-BRAMS.

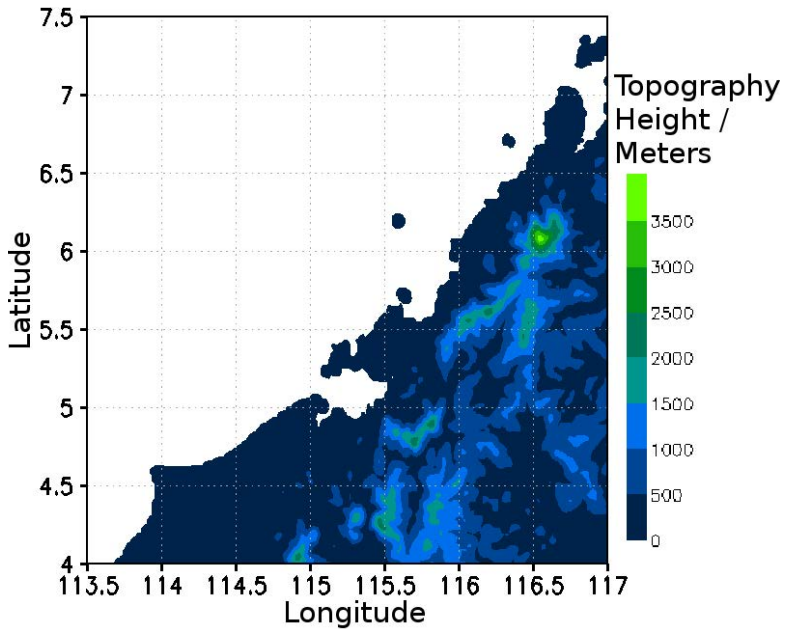

Fig. 6. Map of topography used in CCATT-BRAMS for the finest scale model grid.

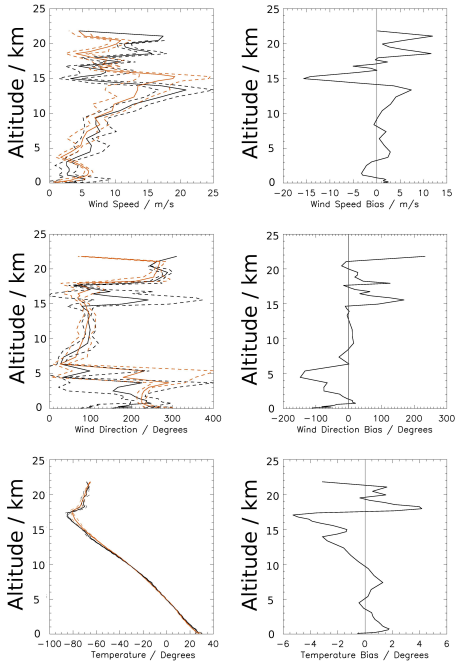

Fig. 7. Comparison between averaged meteorological variables observed above Kuching during the three day simulation and the model output interpolated to the correct time and space. The back line shows the sonde observation data and the orange line shows the model data. Kuching lies within the secondary model grid, which has a spatial resolution of 10 km × 10 km.

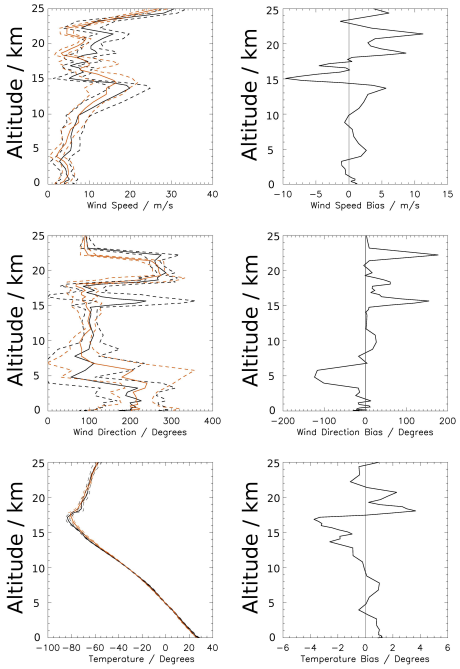

Fig. 8. Comparison between averaged meteorological variables observed above the Sonne RV voyage track during the three day simulation and the model output interpolated to the correct time and space. The back line shows the sonde observation data and the orange line shows the model data. The ship voyage track lies within the secondary model grid, which has a spatial resolution of 10 km × 10 km.

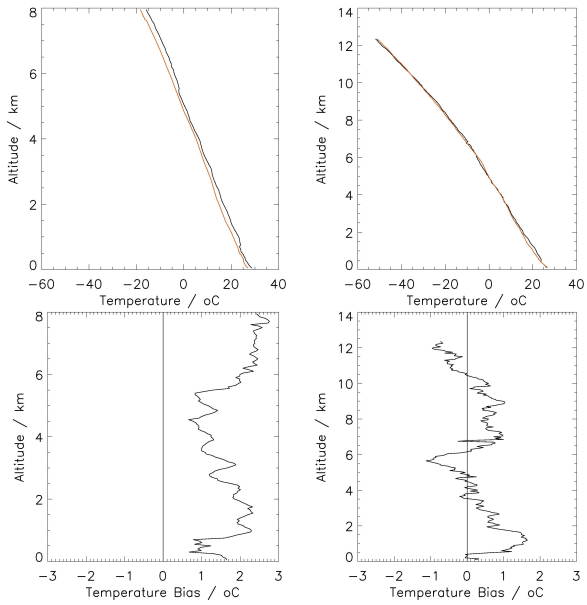

Fig. 9. Comparison between the average observed temperature vertical profiles during both Flights A and B and the model output interpolated to the aircraft track. The left hand figures show the comparison with Flight A, and the right hand figures the comparison with Flight B. The back line shows the sonde observation data and the orange line shows the model data. Flight A was compared to the secondary model grid (spatial resolution 10 km × 10 km), and Flight B to the finest model grid (spatial resolution 2 km × 2 km).

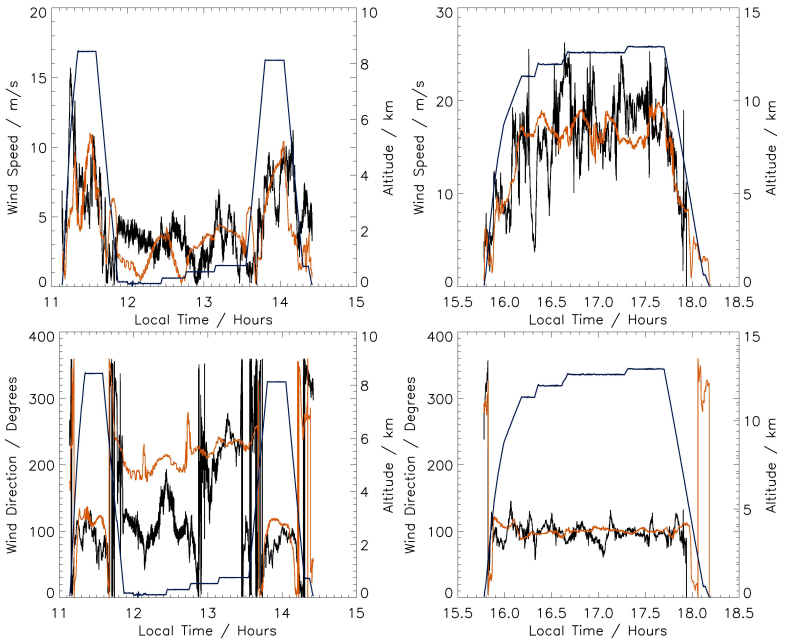

Fig. 10. Comparison between the observed wind speed and direction during both Flights A and B and the model output interpolated to the aircraft track. The left hand figures show the comparison with Flight A, and the right hand figures the comparison with Flight B. The back line shows the sonde observation data and the orange line shows the model data. Flight A was compared to the secondary model grid (spatial resolution 10 km × 10 km), and Flight B to the finest model grid (spatial resolution 2 km × 2 km).

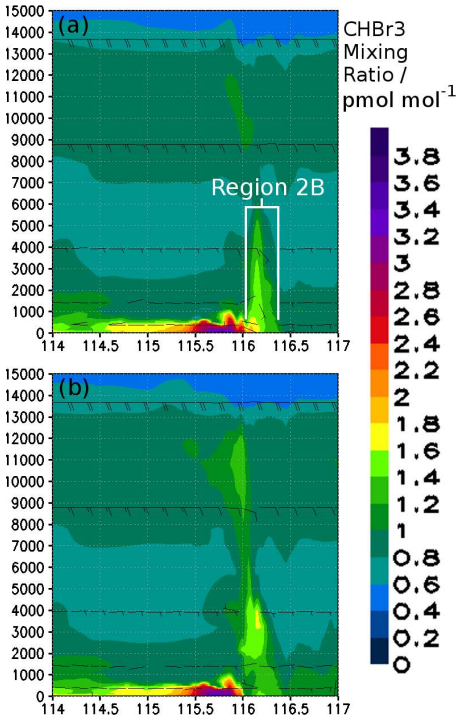

Fig. 11. A sequence of modelled cross sections of the vertical $CHBr_3$ distribution along 5°30′ N during the convective episode that occurred in Region 2B. The y-axis shows the altitude in meters and the x-axis shows the longitude. The wind vectors in this plane are shown with the barbs. The top panel is **(a)** at 15:00 LT, and the middle panel **(b)** is at 16:00 LT.

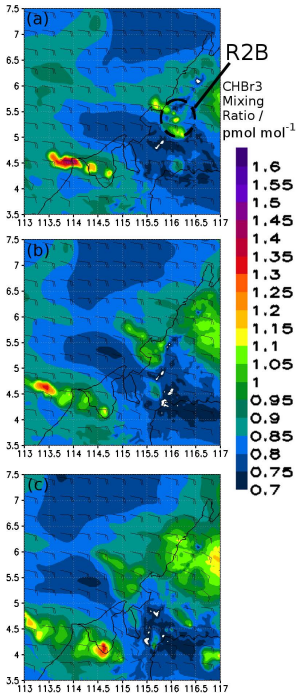

Fig. 12. Simulated $CHBr_3$ mixing ratios at 12 km on 19 November during a portion of Flight B showing the lofting of $CHBr_3$ and its transport from Region 2B to the West. Plot **(a)** is from 16:00 LT, plot **(b)** from 17:00 LT, and plot **(c)** from 18:00 LT. The convective event that lofted $CHBr_3$ at Region 2B in this figure is the same event shown in Fig. 11. The y-axis shows the latitude and the x-axis shows the longitude. The wind vectors at 12 km are shown in addition to the the location of Region 2B.

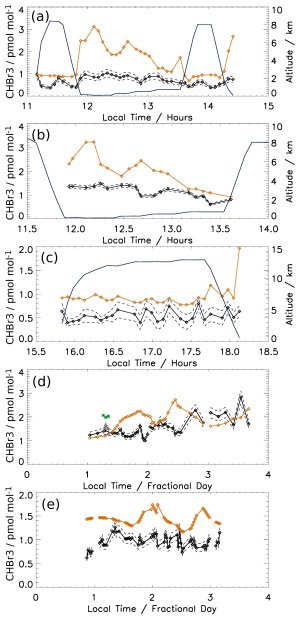

Fig. 13. A comparison between simulated and observed $CHBr_3$. Figure **(a)** is from Flight A (GHOST), Fig. **(b)** from Flight A (WASP), Fig. **(c)** from Flight B (GHOST only), Fig. **(d)** from the Sonne RV and local boat cruises, and Fig. **(e)** from the observations made at Danum Valley. The simulated observations are shown in orange and the observed in black with exception to Fig. **(d)** where, in addition, grey indicates the local boat data and green the corresponding model results. The blue line indicates the height of the Falcon flight. There are additional uncertainties of the observations of $CHBr_3$ due to the accuracy to which the concentration in the standard is known: **(a)** and **(c)** 16.5 %, **(b)** 5 %, and **(e)** 10 %. In the case of **(d)** and **(e)**, zero time corresponds to 00:00 LT 17 November 2011.

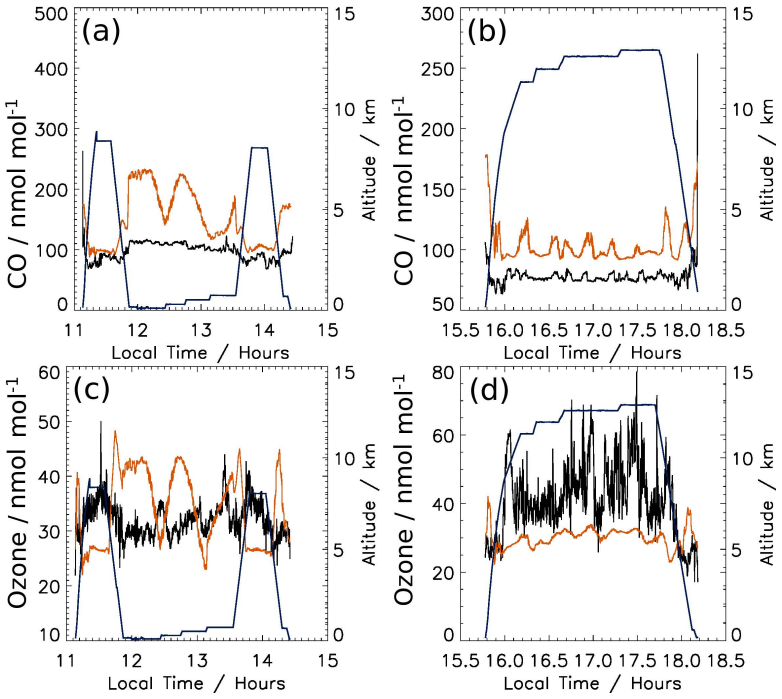

Fig. 14. A comparison between observed and modelled CO and O_3. CO was observed by the SPIRIT instrument and O_3 by the UV-O_3 instrument. Figure (**(a)**, top left) shows the CO during Flight A, Fig. (**(b)**, top right) shows the CO during Flight B, Fig. (**(c)**, bottom left) shows the O_3 during Flight A, and Fig. (**(d)**, bottom right) shows the ozone during Flight B. The simulated mixing ratios are shown in orange and the observed mixing ratios in black. The blue line indicates the height of the Falcon flight.

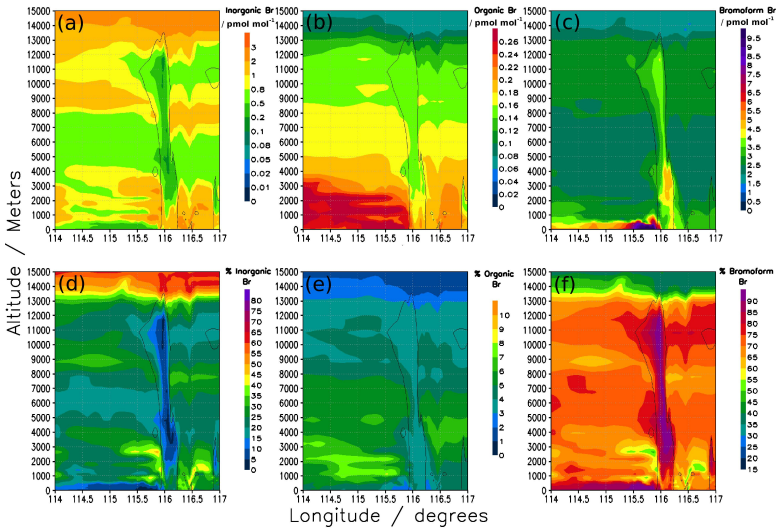

Fig. 15. Simulated vertical cross sections of the mixing ratios and relative contributions to the total simulated bromine atom budget. The cross section intersects a latitude of 5°30′ N at 16:00 LT on 19 November 2011. Figure **(a)** shows the total inorganic bromine (Br, Br_2, BrO, HOBr, HBr, and $BrONO_2$), Fig. **(b)** the total organic bromine ($Br_2C(=O)$, $HBrC(=O)$, $CHBr_2OOH$, and CBr_3OOH), Fig. **(c)** the total amount of bromine atoms from bromoform, Fig. **(d)** the relative contribution of inorganic bromine (Br, Br_2, BrO, HOBr, HBr, and $BrONO_2$), Fig. **(e)** the relative contribution of organic bromine ($Br_2C(=O)$, $HBrC(=O)$, $CHBr_2OOH$, and CBr_3OOH), and Fig. **(f)** the relative contribution of bromine atoms from bromoform. Note that in plots **(a)** and **(d)** the inorganic PG budget includes HBr and HOBr dissolved in cloud particles and rain. Also, in plots **(d)**, **(e)**, and **(f)** the dissolved HBr and HOBr are considered in the relative budget shown in each plot. The y-axis shows the altitude in meters and the x-axis shows the longitude.

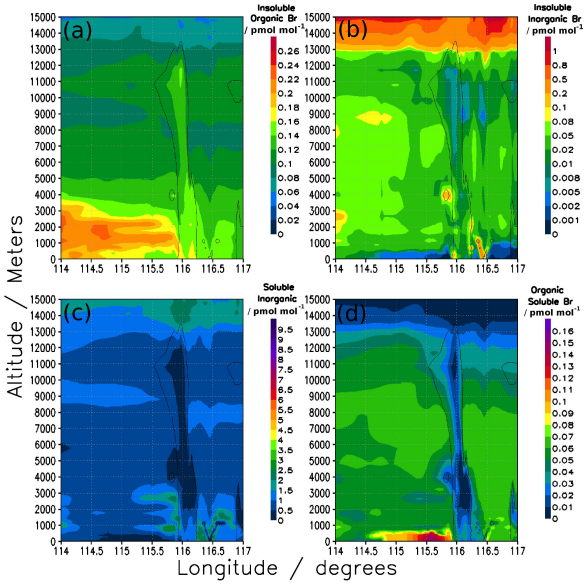

Fig. 16. Simulated vertical cross sections of the mixing ratios of various bromine containing species across a latitude of 5°30′ N during the peak of convective activity at Region 2B at 16:00 LT. Figure **(a)** shows the total of bromine atoms as insoluble organic bromine, **(b)** shows the total bromine atoms as insoluble inorganic bromine, **(c)** shows the total bromine atoms as soluble inorganic bromine, and **(d)** shows the total bromine atoms as soluble organic bromine. Note that the dissolved HBr and HOBr as not included in the budget shown in plot **(c)**. The y-axis shows the altitude in meters and the x-axis shows the longitude.

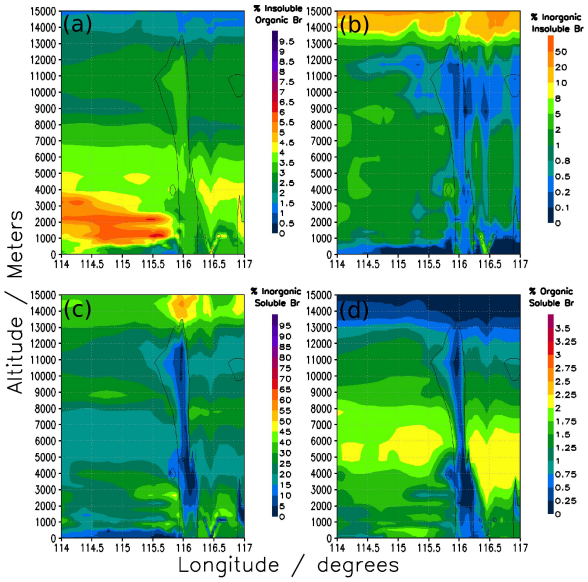

Fig. 17. Simulated vertical cross sections of the relative contributions of various bromine containing species to the total bromine atom budget across a latitude of 5°30′ N during the peak of convective activity at Region 2B at 16:00 LT. Figure **(a)** shows the relative contribution from bromine atoms present as insoluble organic bromine, **(b)** shows the relative contribution from inorganic insoluble, **(c)** the relative contribution from inorganic soluble, and **(d)** the relative contribution from organic soluble bromine. Note that the dissolved HBr and HOBr as not included in the calculation of any of the budgets shown here. The y-axis shows the altitude in meters and the x-axis shows the longitude.

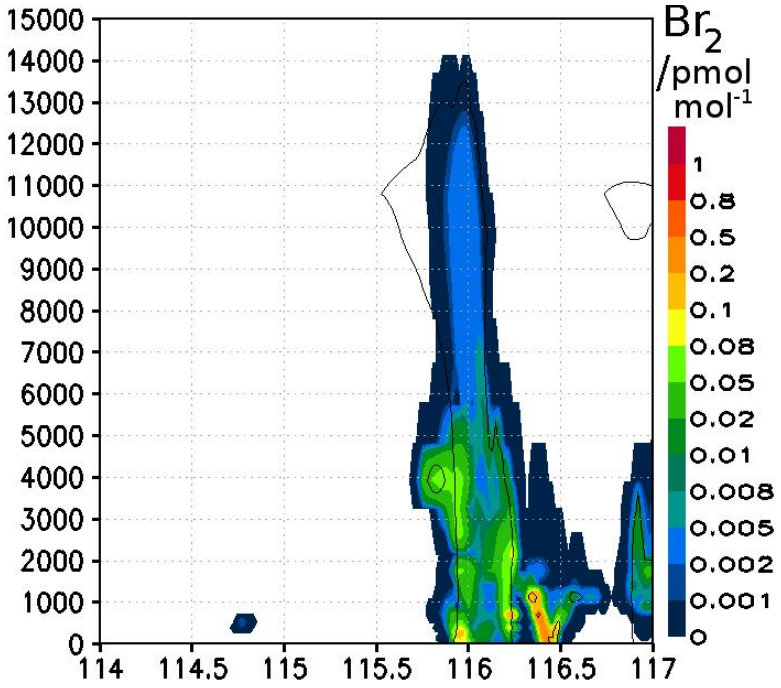

Fig. 18. Simulated vertical cross sections of Br2 across a latitude of 5°30′ N during the peak of convective activity at Region 2B at 16:00 LT.